



# A new species of *Maomingosuchus* from the Eocene of the Na Duong Basin (northern Vietnam) sheds new light on the phylogenetic relationship of tomistomine crocodylians and their dispersal from Europe to Asia

Tobias Massonne, Felix J. Augustin, Andreas T. Matzke, Erich Weber & Madelaine Böhme

To cite this article: Tobias Massonne, Felix J. Augustin, Andreas T. Matzke, Erich Weber & Madelaine Böhme (2022): A new species of *Maomingosuchus* from the Eocene of the Na Duong Basin (northern Vietnam) sheds new light on the phylogenetic relationship of tomistomine crocodylians and their dispersal from Europe to Asia, Journal of Systematic Palaeontology, DOI: [10.1080/14772019.2022.2054372](https://doi.org/10.1080/14772019.2022.2054372)

To link to this article: <https://doi.org/10.1080/14772019.2022.2054372>



© 2022 The Author(s). Published by Informa UK Limited, trading as Taylor & Francis Group.



[View supplementary material](#)



Published online: 18 May 2022.



[Submit your article to this journal](#)



[View related articles](#)



[View Crossmark data](#)



# A new species of *Maomingosuchus* from the Eocene of the Na Duong Basin (northern Vietnam) sheds new light on the phylogenetic relationship of tomistomine crocodylians and their dispersal from Europe to Asia

Tobias Massonne<sup>a,b,\*</sup> , Felix J. Augustin<sup>b</sup> , Andreas T. Matzke<sup>b</sup>, Erich Weber<sup>c</sup> and Madelaine Böhme<sup>a,b</sup>

<sup>a</sup>Senckenberg Center of Human Evolution and Palaeoecology, Tübingen, Germany; <sup>b</sup>Department of Geosciences, Eberhard-Karls-Universität Tübingen, Tübingen, Germany; <sup>c</sup>Institute for Evolution and Ecology, Eberhard-Karls-Universität Tübingen, Tübingen, Germany

(Received 28 September 2021; accepted 14 March 2022)

*Maomingosuchus acutirostris* sp. nov. is a new tomistomine crocodile from the middle–upper Eocene deposits (late Bartonian–Priabonian age, 39–35 Ma) of the Na Duong Basin in northern Vietnam. *M. acutirostris* can be differentiated from the type species *Maomingosuchus petrolicus* by having an acute anterior tip of the premaxilla. Both species differ from another *Maomingosuchus* from Krabi (Thailand) by differences in the surangular–dentary suture and maxillary alveoli. According to our phylogenetic results, *M. acutirostris* seems to be the sister species to the group *M. petrolicus* + Krabi-*Maomingosuchus*. The close relationship between those three tomistomines is supported in the present phylogenetic analysis by three synapomorphies. In our phylogenetic analysis, *Maomingosuchus* was retrieved in a basal position forming the sister group to *Paratomistoma* + *Gavialosuchus* + *Melitosaurus* + *Tomistoma*, including the extant *Tomistoma schlegelii*. This phylogeny indicates three different dispersal events of Tomistominae from Europe towards eastern Asia: 1) for the stem lineage of *Maomingosuchus*, no later than the late Eocene; 2) for the stem lineage of *Penghusuchus pani* + *Toyotamaphimeia machikanensis*, no later than the early–middle Miocene; and (3) for the stem lineage of *T. schlegelii*, during the Neogene.

<http://zoobank.org/urn:lsid:zoobank.org:pub:19B27C1E-0A3F-4425-AA8C-F904277DF327>

**Keywords:** Eocene; Crocodylia; Asia; phylogeny; biogeography

## Introduction

The subfamily Tomistominae is commonly regarded as a monophyletic clade of crocodiles (e.g. Brochu 2007; Jouve 2016; Shan *et al.* 2017; Nicholl *et al.* 2020; but see Lee & Yates 2018; Iijima & Kobayashi 2019; Rio & Mannion 2021; Darlim *et al.* 2022) with only one living representative, the false gharial *Tomistoma schlegelii* (Müller, 1838) from the Malaysian Peninsula, Borneo, Sumatra and Java (Bezuijen *et al.* 2010). Their fossil record is much more diverse, with representatives found in Europe, Africa, America, Asia and Australia (Jouve *et al.* 2015; Jouve 2016; Kuzmin & Zvonok 2021; Ristevski *et al.* 2021). Previous studies suggested that Tomistominae originated in the upper Paleocene to lower Eocene in the region around western Tethys (e.g. Brochu 2007; Piras *et al.* 2007; Jouve *et al.* 2015; Jouve 2016; Shan *et al.* 2017; Martin *et al.* 2019), but the position of basal species differs between studies. *Marccosuchus zennaroi* Jonet & Wouters, 1977 was retrieved as the most basal taxon by several recent studies (Jouve *et al.* 2015; Jouve 2016; Shan *et al.* 2017;

Nicholl *et al.* 2020), whereas a polytomy between *Marccosuchus*, *Kentisuchus* and, if included, *Xaymacachampsia kugleri* (Berg, 1969) was recovered by others (Jouve *et al.* 2015; Iijima *et al.* 2018; Iijima & Kobayashi 2019; Martin *et al.* 2019; Nicholl *et al.* 2020).

During the early and middle Eocene, the tomistomine crocodiles lived in central and southern Europe (*Dollosuchoides densmorei* Brochu, 2007 and *Megadontosuchus arduini* [de Zigno, 1880]), northern Africa (*Tomistoma cairensis* Müller, 1927 and *Paratomistoma courti* Brochu & Gingerich, 2000) and even Central America (*Xaymacachampsia sensu* Jouve *et al.* 2015 and Jouve 2016). Slightly younger, during the middle–upper Eocene, the first undisputed tomistomines are known from Asia (Shan *et al.* 2017; Iijima *et al.* 2018; Martin *et al.* 2019; Nicholl *et al.* 2020). All other tomistomines from eastern Asia are Miocene and Pleistocene in age (*Toyotamaphimeia machikanensis* [Kobatake, ChiJi, Ikebe, Ishida, Kamei, Nakaseko & Matsumoto, 1965]) and *Penghusuchus pani* Shan, Wu,

\*Corresponding author. Email: [tobias.massonne@uni-tuebingen.de](mailto:tobias.massonne@uni-tuebingen.de)

Cheng & Sato, 2009) (Kobayashi *et al.* 2006; Shan *et al.* 2009; Iijima *et al.* 2018).

*Maomingosuchus petrolicus* (Yeh, 1958) was described based on a fragmentary skull. Later, a partially preserved individual was described by Li (1975), based on new material from the Youganwo Formation of the Maoming Basin; Shan *et al.* (2017) later provided a re-description of this material. Recently, another *Maomingosuchus* from Wai-Lek, Krabi Province, Thailand was described by Martin *et al.* (2019). Unfortunately, this specimen is poorly preserved and was provisionally referred to as *Krabi-Maomingosuchus* sp., but it might represent a distinct species.

In this study, we describe a new almost complete species of *Maomingosuchus*, which was excavated in the Na Duong Basin in northern Vietnam in 2011 (Böhme *et al.* 2013) and prepared at the laboratory of the

Geological-Palaeontological Institute of the Eberhard Karls University of Tübingen (GPIT). The new species allows novel insights into the anatomy of *Maomingosuchus*. We incorporated these new data in an expanded phylogenetic analysis of Tomistominae, retrieving a more basal position for *Maomingosuchus* than previously suggested (Shan *et al.* 2017; Iijima *et al.* 2018; Martin *et al.* 2019; Nicholl *et al.* 2020).

## Geological setting

The Na Duong Basin is located in northern Vietnam near the Chinese border (Fig. 1). It represents one of the few areas in eastern and south-eastern Asia with a complete sequence of continental sediments from the middle Eocene–lower Oligocene (Böhme *et al.* 2013). The basin is part of the Cao Bang-Tien Yen fault system and

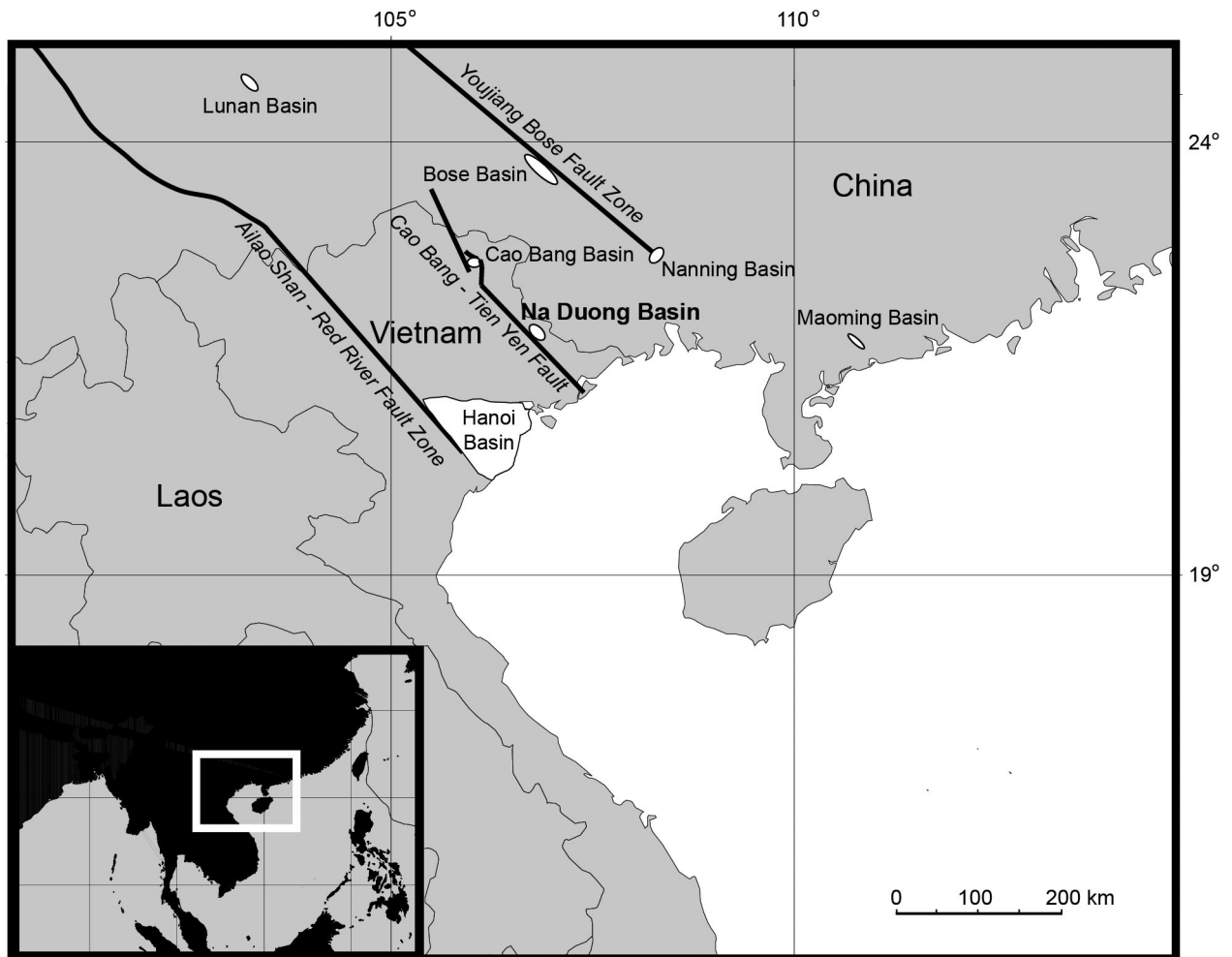


**Figure 1.** Map of the northern part of south-eastern Asia, showing the Na Duong Basin in north-eastern Vietnam close to the border with China (Böhme *et al.* 2013).

covers an area of 45 km<sup>2</sup>. The middle–upper Eocene (late Bartonian–Priabonian, 39–35 Ma) Na Duong Formation is 240 m thick with the upper 140 m of the section being exposed in the Na Duong open cast coal mine.

The tomistomine remains described in this study were found within the transition zone between the coaly shale of the main seam and the underlying dark-brown claystone (layer 80).

The sediments of layer 80 are lacustrine lignitic shales and were deposited during a time of tropical to warm sub-tropical climate. During this time, this region was in a transitional stage from an environment characterized by shallow ponds to a large anoxic lake environment (Böhme *et al.* 2013; Garbin *et al.* 2019). The ecosystem yielded both aquatic and terrestrial faunal elements. The new tomistomine *Maomingosuchus acutirostris* occurred sympatrically with *Orientalosuchus naduongensis* Massonne, Vasilyan, Rabi & Böhme, 2019, members of Cetartiodactyla and Perissodactyla, many fish and two turtle species (Böhme *et al.* 2013; Garbin *et al.* 2019). While the majority of aquatic specimens were found articulated, the terrestrial mammals were preserved disarticulated (Garbin *et al.* 2019).

## Materials and methods

All of the herein described material belongs to one individual GPIT-PV-31657, which was found at the base of layer 80 (*sensu* Böhme *et al.* 2011) in the Na Duong coal mine. The bones were disarticulated and dispersed over a small area of around 4 m<sup>2</sup>. Since all of the bones were found in close proximity, and are of the same general size with no duplication of elements, it is clear that GPIT-PV-31657 represents a single individual. The material consists of a skull with articulated mandibles as well as the almost complete disarticulated postcranial material. The skull is dorsolaterally compressed, so the ventral and occipital regions are poorly preserved. The disarticulated vertebral column consists of the proatlas, seven cervical, 12 dorsal, two sacral and 15 caudal vertebrae, as well as multiple chevrons. Of the ribs, a single atlantal rib, seven cervical ribs and nine dorsal ribs are preserved. Both scapulae and coracoids are also preserved as well as both humeri and a single ulna, while the radius, the metacarpals and the manual phalanges are missing. Also preserved are both ilia, ischia and pubes, both femora, a single tibia and fibula, as well as four metatarsals, whereas all pedal phalanges are missing. Osteoderms from the dorsal and lateral body sections were found in large numbers.

For our phylogenetic analysis we used the dataset of Nicholl *et al.* (2020) (see [Supplemental material S1](#)), which was the most recent dataset focusing mainly on the relationships of tomistomines. Their dataset is mainly based on Jouve (2016), which is derived from multiple previous datasets including Brochu (1999) and Jouve *et al.* (2015). The focus of our updated phylogeny is to clarify the relationships of *Maomingosuchus* within the family Tomistominae. The species *Maomingosuchus acutirostris* sp. nov. as well as the Krabi-*Maomingosuchus* (Martin *et al.* 2019) were added to the dataset that now consists of 72 taxa and 244 characters. *Bernissartia fagesii* Dollo, 1883 was used as the out-group taxon. For the analysis, we followed Nicholl *et al.* (2020) and retained the 31 ordered characters from that analysis (characters 7, 30, 37, 62, 64, 75, 78, 81, 87, 91, 95, 103, 124, 131, 145, 151, 152, 153, 156, 161, 169, 171, 173, 174, 176, 177, 179, 194, 195, 206, 238). For *M. acutirostris* we scored 111 characters (see dataset in [Supplemental material S1](#)). Character scorings were modified for *Maomingosuchus petrolicus* and the Krabi-*Maomingosuchus* (a complete list of changes and the list of specimens are in [Supplemental material S2](#), while the list of characters is in [Supplemental material S3](#)).

We conducted a maximum parsimony analysis as a ‘traditional’ search in TNT v. 1.5 standard version updated on 31 March 2021 (Goloboff & Catalano 2016). We treated the multistate characters as ordered (see above) and equally weighted; set the maximum of trees to 99,999 and the tree replications to 1000. For the branch swapping algorithm, we used tree bisection reconnection with 10 trees saved per replication. A first run of heuristic search tree-bisection-reconnection failed to find all the most parsimonious trees (MPT) and, therefore, the heuristic search was repeated until the MPTs were found 50 times during each replicate (using the command ‘xmult = hits 50;’), as in Massonne *et al.* (2019). The trees retained in the memory were exposed to a second round of tree-bisection-reconnection.

We also conducted a ‘New Technology’ search due to the large dataset (Goloboff *et al.* 2008). The random addition sequence was set to 1000. For the search algorithm, sectorial search, ratchet and tree fusing were used. For sectorial search in the RSS settings, the maximal sector size was set to 36, representing half of the taxa in the dataset, in the CSS settings the rounds were set to 100 and the minimal sector size to five, and for the XSS settings the number of rounds was set to 10. In the ratchet settings the total number of iterations was set to 100, for tree fusing the rounds were set to 100. All other options were left as default. After the first round, we conducted a second round of new technology search with the trees saved from ram. Sectorial search was

disabled, and we changed the number of iterations in the ratchet settings to 1000 and the tree fusing to 1000 rounds. The result was filtered for sub-optimal trees and the analysis was run again until the number of found trees did not change further.

## Institutional abbreviations

**DM**, Darwin Fossil Museum, Keelung, Taiwan; **GPIT** Geologisch-Paläontologisches Institut Tübingen, Tübingen, Germany; **NMNS** National Museum of Natural Science, Taichung, Taiwan.

## Systematic palaeontology

**Eusuchia** Huxley, 1875 *sensu* Brochu 2003

**Crocodylia** Gmelin, 1789 *sensu* Benton & Clark 1988

**Crocodyloidea** Fitzinger, 1826 *sensu* Brochu 2003

**Tomistominae** Kälin, 1955 *sensu* Brochu 2003

***Maomingosuchus*** Shan *et al.*, 2017

**Emended genus diagnosis.** *Maomingosuchus* is diagnosed by the unique combination of the following characters: 1) distinct dorsoventrally extending ridges on the lateral and mesial surfaces of the anterior teeth (shared with an indeterminate tomistomine from the Ikovo locality and some non-tomistomine taxa); 2) presence of a frontal fossa between the orbits, close to the posterior end of the prefrontals (shared with ‘*Crocodylus*’ *affinis* Marsh, 1871 and *Prodiplocynodon langi* Mook, 1941); 3) a flat frontal margin between the orbits (shared with *Dollosuchoides*). Only preserved in *Maomingosuchus acutirostris* and *Maomingosuchus petrolicus* are: 4) perforations for the first dentary tooth anterior to the external naris (shared with *Kentisuchus spenceri* [Buckland, 1836]); 5) 15 maxillary teeth in total (shared with *Dollosuchoides*); and (6) exoccipital with ventrally projecting lamina hiding the entrance to the cranio-quadrate passage (shared with gharials and basal eusuchians).

***Maomingosuchus acutirostris*** sp. nov.

(Figs 2–14)

**Diagnosis.** *M. acutirostris* is a medium-sized tomistomine with a skull length (premaxilla–supraoccipital) of 546 mm and an estimated total length of around 3.5 m based on the skull to body length ratio of extant *Tomistoma schlegelii* (1:6.4 according to Whitaker & Whitaker 2008), which presumably has similar body proportions. It can be diagnosed by the combination of

the following characters: 1) relatively robust teeth, especially the 5th maxillary tooth and the 11th or 12th dentary teeth (similar to *Marccosuchus*); 2) anterior part of the prefrontal on the same level as anterior part of the frontal (shared with the Krabi-*Maomingosuchus*, some individuals of *Maomingosuchus petrolicus* and *Gavialosuchus eggenburgensis* [Toula & Kail, 1885]); 3) supraoccipital visible on dorsal skull table (shared with ‘*Tomistoma*’ *cairensis*, ‘*Tomistoma*’ *coppense*, *Paratomistoma* and *M. petrolicus*); 4) atlantal rib with process on dorsal margin (shared with *Toyotamaphimeia* and some non-tomistomines); and 5) ilium with a prominent anterior process (shared with *Penghusuchus* and *Toyotamaphimeia*).

Beside the characters mentioned above, *M. acutirostris* can be further differentiated from *M. petrolicus* by: having an elongated premaxilla, anterior to the external naris; a ratio of the mediolateral width of the supratemporal fenestral bar to the width of the skull table at the same level of 0.100–0.175, and a ratio of the anteroposterior length of supratemporal fenestra to the anteroposterior length of the orbit >0.75.

Both *M. acutirostris* and *M. petrolicus* can be differentiated from the Krabi-*Maomingosuchus* by: having the first five maxillary teeth getting continuously larger posteriorly; the 7th and 8th maxillary teeth more widely spaced than other teeth; a ratio of the anteroposterior length of the supratemporal fenestra to the anteroposterior length of the orbit >0.75 and a surangular–dentary suture intersecting the external mandibular fenestra anterior to its posterior corner.

**Etymology.** The species name derives from the Latin word *acutus* for ‘acute’ and *rostrum* for ‘snout’ and refers to the elongated acute premaxilla anterior to the external naris, which stands in a marked contrast to the short and rounded premaxilla of *M. petrolicus*.

**Holotype.** GPIT-PV-31657, partial skeleton consisting of the complete skull, lower jaw and incomplete postcranial material (see [Supplemental material S4](#) for a complete list of the material).

**Type locality and horizon.** The fossil was recovered from layer 80 of the Na Duong coal mine (Böhme *et al.* 2013) in northern Vietnam (21°42.2’N, 106°58.6’E); Na Duong Formation, Eocene, late Bartonian–Priabonian age (39–35 Ma).

**Remarks.** Martin *et al.* (2019) described a *Maomingosuchus* sp. from the upper Eocene–lower Oligocene Wai-Lek Formation from Krabi Province, Thailand based on a partly preserved skull and lower jaw. The authors refrained from erecting a new species for the Krabi-*Maomingosuchus* due to its fragmentary preservation and the overall similarity with *Maomingosuchus petrolicus*. In our analysis, the Krabi-*Maomingosuchus* was found to be

closely related to *M. petrolicus*, but with three autapomorphies distinguishing it from the other maomingosuchids: 1) a surangular–dentary suture that intersects the external mandibular fenestra at its posterior corner (character [ch.] 65-1); 2) from the 1st to the 10th maxillary alveolus only one tooth larger, the others being of nearly same size (ch. 203-1); and 3) maxillary teeth widely spaced and the 7th and 8th teeth not more widely spaced than other teeth (ch. 235-1). We therefore treat the Krabi-*Maomingosuchus* as a provisionally valid

but unnamed species of *Maomingosuchus* (see Discussion, below).

## Description

Overall, the material is well preserved and represents nearly a complete individual. The skull is articulated

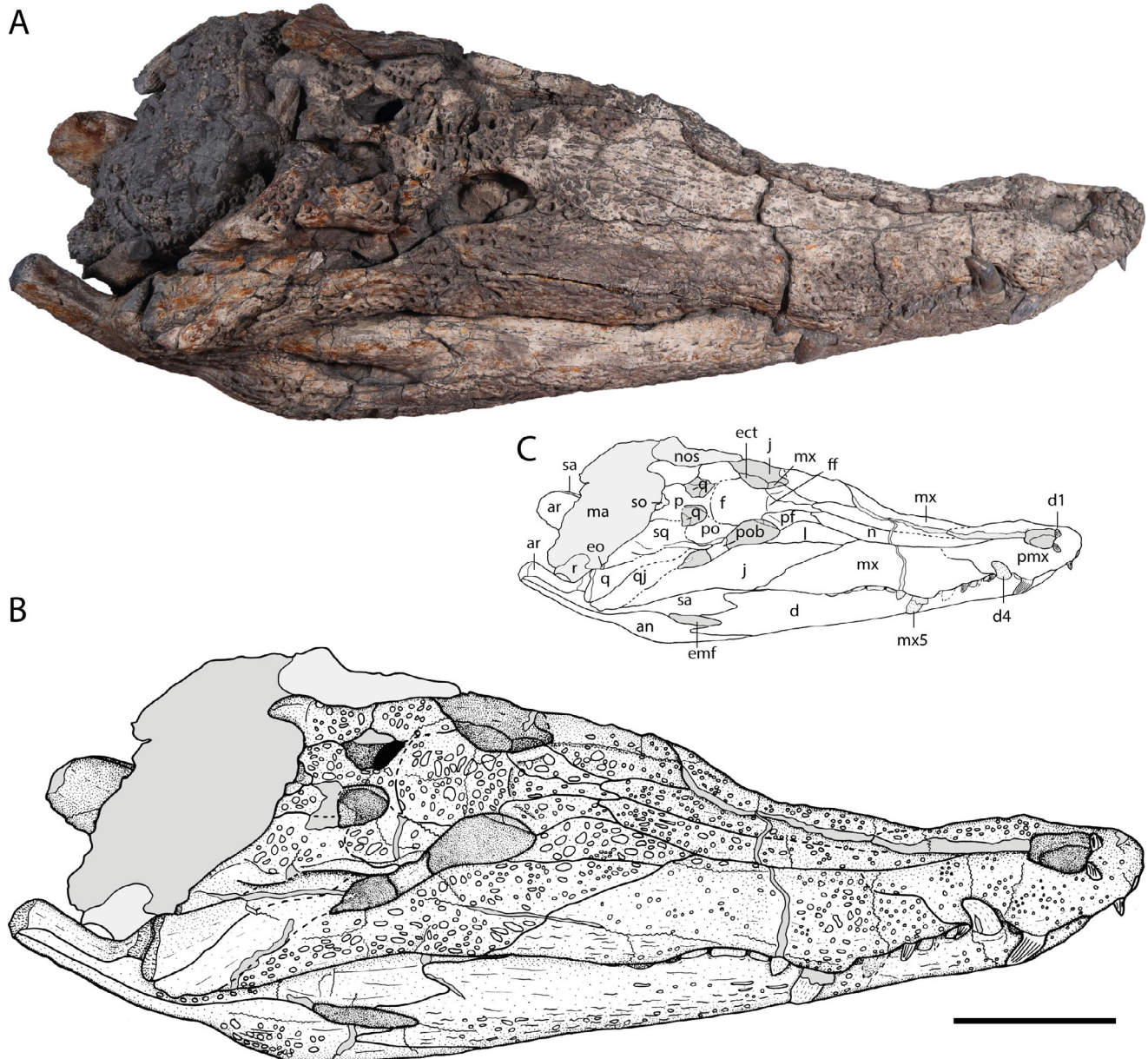


**Figure 2.** *Maomingosuchus acutirostris*, holotype, GPIT-PV-31657, Na Duong Formation, middle to upper Eocene, Vietnam. Skull in **A**, **B**, dorsolateral view and **C**, a sketch with the visible bones and characteristics. **Abbreviations:** **an**, angular; **ar**, articular; **d**, dentary; **d1**, dentary tooth 1; **d4**, dentary tooth 4; **ect**, ectopterygoid; **emf**, external mandibular fenestra; **eo**, exoccipital; **f**, frontal; **ff**, frontal fossa; **j**, jugal; **l**, lacrimal; **ma**, matrix; **mx**, maxilla; **mx5**, maxillary tooth 5; **n**, nasal; **nos**, nuchal osteoderm; **p**, parietal; **pf**, prefrontal; **pmx**, premaxilla; **po**, postorbital; **pob**, postorbital bar; **q**, quadrate; **qj**, quadratojugal; **r**, rib; **sa**, surangular; **so**, supraoccipital; **sq**, squamosal. Scale bar = 10 cm.

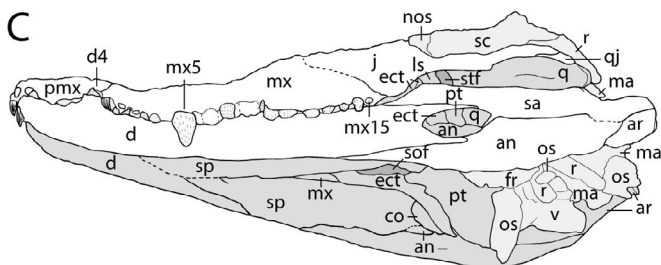
with the lower jaw and dorsolaterally flattened. The posterior part of the skull is still covered in matrix. The postcranial material is disarticulated and preserved three dimensionally with only minor compression artefacts. Most of the bones are pyritized.

For measurements of the cranial and postcranial material see [Supplemental material S4](#).

## Cranial bones

**General shape and taphonomic remarks.** The skull is relatively robust, with the snout (measured from the snout tip to the anterior margin of orbit) making up around 72% of total skull length. The snout is overall

A



B

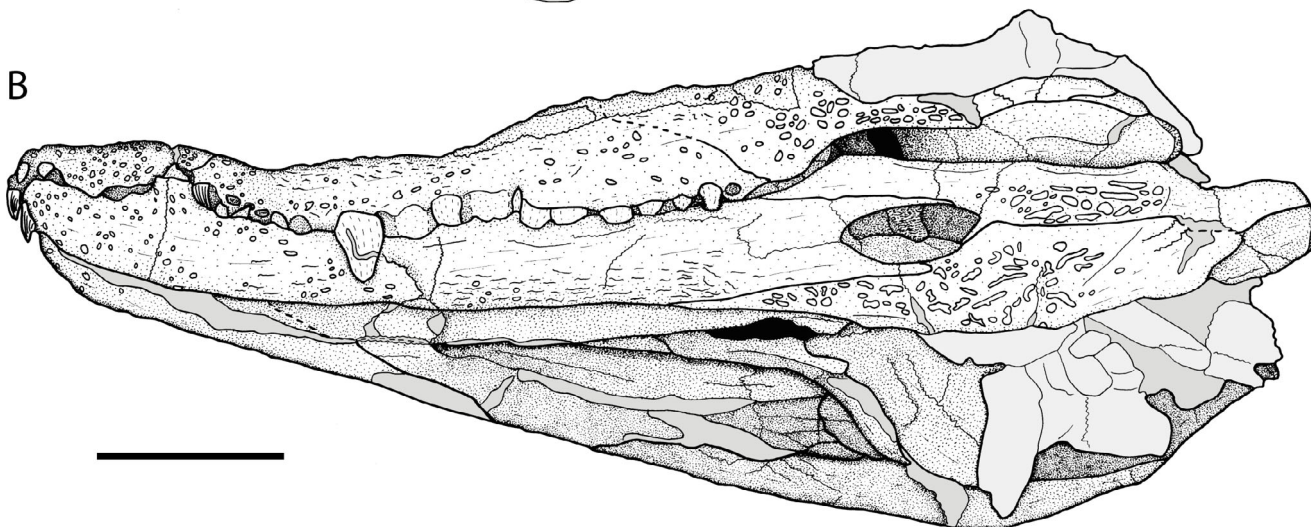


**Figure 3.** *Maomingosuchus acutirostris*, holotype GPIT-PV-31657, Na Duong Formation, middle to upper Eocene, Vietnam. Skull in **A**, **B**, ventrolateral view and **C**, a sketch with the visible bones and characteristics. **Abbreviations:** an, angular; ar, articular; co, coronoid; d, dentary; d4, dentary tooth 4; ect, ectopterygoid; fr, fragment; j, jugal; ls, laterosphenoid; ma, matrix; mx, maxilla; mx5, maxillary tooth 5; mx15, maxillary tooth 15; nos, nuchal osteoderm; os, osteoderm; pmx, premaxilla, pt, pterygoid; q, quadrate; qj, quadratojugal; r, rib; sa, surangular; sc, scapula; sof, suborbital fenestra; sp, splenial; stf, supratemporal fenestra; v, vertebra. Scale bar = 10 cm.

narrow but widens at the level of the 5th maxillary tooth. The skull table is solid with relatively small supratemporal fenestrae and a wide frontal region between the orbits. The postorbital bar is very robust. The skull is highly pyritized and cracked in multiple regions; for example, posterior to the external naris, the region of the skull table and the otic region. The skull is articulated with the lower jaw and dorsolaterally compressed, so that most of its ventral surface is obscured. The occiput is partly embedded in matrix together with some postcranial elements. Most cranial features described below can be seen in [Figures 2 and 3](#).

**Cranial openings.** The external naris ([Fig. 2](#)) is a large singular opening in the anterior region of the snout and formed exclusively by the premaxillae. Due to mediolateral compression of the skull the exact shape of the external naris is difficult to assess, but it seems to be trapezoidal and broader anteriorly than posteriorly. Both orbits ([Fig. 2](#)) are preserved, but only the right one is well exposed and is oriented dorsolateral and almost oval, but slightly lateromedially compressed. Its margins are formed by the lacrimal, prefrontal, frontal, post-orbital and jugal. Both supratemporal fenestrae ([Fig. 2](#)) are visible, lie on the skull table, and are small for a tomistomine. The outlines of the fenestrae are difficult to determine due to some broken areas and compression but they seem to be rounded and slightly longer than broad. Their medial walls are smooth without any visible foramina, and their margins are formed by the post-orbitals, squamosals and parietals. Only the right infratemporal fenestra ([Fig. 2](#)) is visible posterior to the orbits. It is triangular in shape and enclosed by the post-orbital, jugal and quadratojugal. Only the left suborbital fenestra ([Fig. 3](#)) is exposed in ventral view, bordered by the ectopterygoid and pterygoid so far as visible. Both external mandibular fenestrae ([Figs 2, 3](#)) are preserved and lie in the posterolateral region of the lower jaw. They are oval and anteroposteriorly elongated. Their margins are formed by the dentaries, angulars and sur-angulars. The incisive foramen, posttemporal foramen, foramen magnum, eustachian opening, choana and the foramen intermandibularis caudalis are not exposed.

**Premaxilla.** The right premaxilla is better preserved than the left. The premaxillae form the anterior part of the snout and entirely surround the external naris. Their surface is weakly ornamented. Close to the tooth row, small, rounded foramina for the receptor canals are exposed. The premaxilla projects anterior to the external naris for around half of narial length and forms the acute tip of the snout. In front of the external naris a perforation for the first dentary tooth is visible. The premaxilla extends posterior to the level of the 3rd

maxillary tooth, presumably reaching the level of the posterior border of the 4th maxillary tooth parasagittally. Both premaxillae meet each other anterior to as well as posterior to the external naris. The premaxillary–maxillary suture extends as a sinusoidal line from the notch for the 4th dentary tooth posteromedially. The premaxilla contacts the nasal behind the external naris. Only one large tooth is visible, which can be identified as the 4th premaxillary tooth, based on comparisons with other tomistomines. Taking the length of the premaxilla into account a total of five premaxillary teeth is estimated.

**Maxilla.** The maxilla forms the posterolateral part of the snout, most of the tooth row and terminates about 15 mm posterior to the last tooth. It is weakly ornamented with a higher density of pits and grooves on the level between the 3rd and 5th maxillary tooth. Along the tooth row, openings for the receptor canals can be observed. These foramina are rounded anteriorly and get more elongated posteriorly. In dorsal view, the maxilla broadens slightly from the notch for the 4th dentary tooth towards the level of the 5th maxillary tooth, narrowing again at level of the 7th to 8th maxillary tooth, before bending posterolaterally. The maxilla sutures with the nasal medially, the lacrimal posteromedially, the jugal posteriorly and the ectopterygoid posteroventrally. The maxilla has a total of 15 alveoli. The 1st maxillary alveolus is the smallest. The teeth then increase in diameter until the 5th maxillary tooth, which is the largest in the series. The teeth become slightly smaller posteriorly, but stay relatively large, except for the last four which are significantly smaller than the previous ones. The alveoli are widely spaced ([Fig. 2](#)), especially among the smaller anterior teeth, whereas the larger posterior teeth are closer together. Between the 7th and 8th maxillary teeth there is a wider gap.

**Nasal.** The nasals are thin, elongate bones forming the medial part of the snout. Their anterior-most part is not clearly visible but it is definitely excluded from the external naris. The nasal surface is only weakly ornamented anteriorly, but more strongly so posteriorly with rounded and elongated pits. The nasal contacts the premaxilla anteriorly, the maxilla laterally and the lacrimal posterolaterally. Posteriorly, the nasal sutures with the prefrontal for a short distance (only 20 mm), whereas posteromedially they are separated by a 15 mm long anterior process of the frontal.

**Lacrimal.** Only the right lacrimal is well preserved. The bone is elongated anteroposteriorly, slightly bowed medially and forms the anterolateral margin of the orbit. The bone is almost double the size of the prefrontal and projects far anteriorly between the nasal and maxilla. Its surface is heavily ornamented with large rounded pits. The opening for the ductus nasolacrimalis is not

exposed. The lacrimal contacts the maxilla anterolaterally, the jugal laterally, the prefrontal medially and the nasal anteromedially.

**Prefrontal.** The prefrontal forms the anteromedial margin of the orbit. The bone is almost rectangular and does not project further anteriorly than the anterior end of the frontal and is approximately as broad as the lacrimal. The orbital margin has a small bulge extending medially onto the frontal fossa. The surface of the prefrontal is weakly ornamented with a few deeper pits posteriorly. Due to crushing of the skull, neither prefrontal pillars is preserved. The prefrontal contacts the nasal anteriorly, the lacrimal laterally and the frontal medially.

**Frontal.** The frontals are fused and form the anterior part of the skull table. The bone is almost square-shaped with an elongate anterior wedge-shaped process, which projects with its anterior-most extension between the nasals. The whole process has nearly the same length as the broad part between the orbits and the skull table. The frontal does not reach the supratemporal fenestra posteriorly. The region between the orbits is flat, not upturned, very broad and around three times wider than the supratemporal bridge. The region between the broader part of the frontal and the narrow region of the anterior process is marked by a lateromedially oriented frontal fossa forming a ledge between the skull table and the snout. This fossa extends anterolaterally onto the prefrontal. The frontal is weakly ornamented anteriorly, but heavily ornamented with deep rounded pits posterior to the ledge. Anteromedially, the frontal contacts the nasal and anterolaterally, the prefrontal. On the skull table, the frontal contacts the postorbital laterally and the parietal posteriorly. The suture with the latter seems to project relatively straight lateromedially, but a slight posteromedial convexity is visible.

**Postorbital.** The right postorbital is the better preserved and forms the anterolateral part of the skull table, the posterolateral margin of the orbit, the anterolateral margin of the supratemporal fenestra and the anterior margin of the infratemporal fenestra. The skull table is damaged and therefore the postorbital is somewhat distorted with its surface partially broken off. The preserved part is ornamented with large rounded pits, especially posteriorly. In dorsal view, the postorbital contacts the frontal anteromedially, the parietal posteromedially and the squamosal posteriorly. In lateral view, the postorbital is indented by an anterior process of the squamosal. The postorbital bar is slightly inset from the margin of the skull table, very robust and is at least 50% the size of the infratemporal fenestra. The sutural contact with the jugal is not visible.

**Parietal.** The flat, dumbbell-shaped parietals are fused at midline and form most of the posteromedial part of the skull table as well as the medial margin of the supratemporal fenestra. The region posterior to the supratemporal fenestra is very broad. The supratemporal bar is narrow, but quite broad for a tomistomine. The parietal surface is ornamented with deep rounded pits. The parietal contacts the frontal anteriorly, the postorbital anterolaterally and the squamosal posterolaterally. The parietal encompasses the supraoccipital in the posterior part of the skull table, so that the parietal does not form the entire skull table. Inside the supratemporal fenestra, the parietal contacts the quadrate along its posterior wall, but the suture is difficult to see.

**Squamosal.** The squamosal is better preserved on the right side, and forms the posterolateral part of the skull table and the posterolateral margin of the supratemporal fenestra. The squamosal prongs extend posterolaterally, away from the skull table. The dorsal and ventral rims of the squamosal groove for the external ear valve musculature are parallel. The squamosal surface is ornamented with rounded pits only in the skull table region. Due to compression, the squamosal completely covers the auditory meatus. On the skull table, the squamosal contacts the postorbital anteriorly, the parietal posterolaterally and the quadrate on the lateral wall of the supratemporal fenestra. In lateral view, the squamosal projects anteriorly into the postorbital and contacts the quadrate posterolaterally on the squamosal prongs. The suture with the exoccipital is poorly preserved, but it is clear that the squamosal does not cover the paroccipital process.

**Jugal.** The right jugal is better preserved than the left and forms the lateral part of the skull as well as the ventrolateral margins of the orbit and the infratemporal fenestra. Anteriorly, a process extends far anteriorly to the level of the anterior extension of the frontal. The jugal is narrowest at level of the postorbital bar. The postorbital bar is set inwards from the lateral part of the skull and separated from it by a deep groove. The entire surface of the jugal is heavily ornamented. The jugal contacts the maxilla anteriorly, the lacrimal medially and the ectopterygoid ventrally. The jugal–quadratojugal suture is somewhat damaged posteriorly and its interaction with the posterior margin of the infratemporal fenestra is unclear. The jugal–postorbital suture on the postorbital bar is not visible.

**Quadratojugal.** The right quadratojugal is the best preserved. The bone is small, situated at the posterolateral part of the skull and forms the posterior margin of the infratemporal fenestra. The quadratojugal extends to the posterior end of the skull, surpassed only by the

quadrate condyles. No surface ornamentation is observable. The quadratojugal contacts the jugal anteriorly and the quadrate posteromedially. A potential contact with the postorbital and squamosal at the superior margin of the infratemporal fenestra is not exposed.

**Quadrate.** The right quadrate is visible in dorsal and posterior views, while the left quadrate is exposed in ventral view only. It forms the posterior-most part of the skull, the inner posterior part of the supratemporal fenestra as well as the articulation with the articular of the lower jaw and most of the margin of the auditory meatus, which is not exposed. The articular surface of the quadrate is formed by two condyles, of which the lateral one is more expanded lateromedially than the medial one. The surface of the bone is unornamented. The quadrate foramen aerum is located in the dorsomedial corner of the bone. The quadrate is broad at the level of the condyles and narrows anteriorly close to the quadratojugal. The ventral surface of the quadrate is generally smooth with a moderate ridge for the insertion of the posterior mandibular adductor muscle. In dorsolateral view, the quadrate contacts the quadratojugal anteriorly, the squamosal medially and the exoccipital posteromedially. Inside the supratemporal fenestra, the quadrate contacts the parietal posteromedially and the squamosal posterolaterally, but this region is poorly preserved. In occipital view, the quadrate contacts the exoccipital dorsally.

**Pterygoid.** The pterygoid is only visible in ventral view where it forms the posterior part of the palate and the posterior margin of the suborbital fenestra. Due to dorsolateral compression, it is poorly preserved and only the left wing of the pterygoid is exposed (Fig. 3). The region around the choana is damaged. The pterygoid contacts the ectopterygoid anterolaterally. Unfortunately, no other sutural contacts are visible.

**Ectopterygoid.** Only the left ectopterygoid is exposed in ventral view. It forms the posterolateral part of the palate and forms the posterolateral margin of the suborbital fenestra. The ectopterygoid is poorly preserved and distorted, but its posterior extension contacts the pterygoid and ends anterior to the posterior tip of the latter. It further contacts the maxilla anteriorly and the jugal dorsally.

**Supraoccipital.** The supraoccipital is an unpaired bone and forms a small part of the skull roof and the central dorsal part of the occiput. On the skull table, it is a small triangular element that is pinched between the parietals. Its surface is somewhat weathered but no surface ornamentation is visible. The occipital part of the bone is damaged due to dorsolateral compression.

**Exoccipital.** The right exoccipital is exposed in occipital view but only its posterolateral-most parts are preserved. It forms most of the posterolateral region of the skull and the paroccipital process is visible in lateral view. The opening for the cranioquadrate passage is not directly visible, but the exoccipital shows a ventrally projecting convexity at the level of the foramen. The exoccipital contacts the squamosal dorsal and the quadrate ventrally. No other sutural contacts are visible.

**Laterosphenoid.** Only the left laterosphenoid is partly exposed and situated on the anteroventral part of the skull table, posteromedial to the orbit. It forms the anterolateral braincase wall and the inner anteromedial wall of the supratemporal fenestra. Sutural contacts with other bones are not discernible.

**Dentary.** Both dentaries are well-preserved in lateral view. The bone covers the anterolateral part of the lower jaw and reaches the anterodorsal and anteroventral part of the external mandibular fenestra. The dentary symphysis is relatively short for a tomistomine and seems to extend back to the level of the 6th to 8th dentary alveolus, although its exact length is difficult to determine due to poor preservation. The surface of the dentary is slightly ornamented with rounded pits anteriorly and elongated grooves ventrally, while its posterodorsal part is almost smooth. The tooth row is almost straight and, close to it, openings for receptor canals are visible. The slight curvature of the dentary, observable on the right side in lateral view (Fig. 2) is most likely a compressional artefact, as it is not present on the left side (Fig. 3). The dentary contacts the surangular posterodorsally, the angular posteroventrally and the splenial posteromedially. The total tooth number is unclear. The 1st dentary tooth perforates the premaxilla immediately anterior to the external naris. The 4th dentary tooth is the largest tooth in the anterior half of the lower jaw and its alveolus is slightly elevated. Posteriorly, the teeth are smaller but the 11th or 12th tooth (estimated based on the distance between the anterior teeth) is very broad and slightly larger than the 4th. Posteriorly, the tooth row is not exposed.

**Splenial.** The left splenial is the best preserved but is somewhat distorted. It forms the posteromedial part of the mandibular symphysis with a length that is less than the distance between five alveoli. An anterior foramen for cranial nerve V is not visible, but this could be a preservational artefact. There is no surface ornamentation. The splenial contacts the dentary laterally, the coronoid posterodorsally and the angular posteroventrally.

**Coronoid.** The left coronoid is exposed medially but is poorly preserved, and only its crescent-shaped anterior

part is visible. Its surface is smooth, with no visible foramina, but this could be an artefact. The coronoid contacts the splenial anteriorly and the angular ventrally. The contact with the surangular is not exposed.

**Surangular.** Both surangulars are preserved in lateral view only. The surangular forms the posterodorsal part of the lower jaw, the posterodorsal margin of the external mandibular fenestra, contributes laterally to the posterior-most end of the retroarticular process, and reaches the dorsal tip of the lateral wall of the glenoid fossa. Anteriorly, the bone has two processes, a longer dorsal one, presumably reaching the tooth row, and a shorter ventral one, extending anteriorly to the external mandibular fenestra for around half of the fenestral length. The surangular is strongly ornamented with deep elongated pits posterior to the external mandibular fenestra. It contacts the dentary anteriorly, the angular ventrally and the articular dorsomedially.

**Angular.** Both angulars are preserved in lateral view and the right one is partially visible in medial view. The angular forms the posteroventral part of the mandible and the posteroventral margin of the external mandibular fenestra. Anteroventrally, the bone forms a process projecting between the dentary and splenial while extending posteriorly alongside the surangular on the lateral wall of the retroarticular process until its posterior-most end. The angular is strongly ornamented on its lateral part with deep and elongated pits, as well as with a few rounded pits posteroventral to the external mandibular fenestra. On its posteroventral part, a small nutritional foramen is visible in ventral view. In lateral view, the angular contacts the dentary anteriorly and the surangular dorsally. In medial view, the angular contacts the splenial anteriorly, the coracoid anterodorsally and the articular posterodorsally. A contact with the surangular in medial view is not exposed.

**Articular.** Both articulars are preserved in dorsolateral view and the right one is partially visible in medial view. The articular forms the posteromedial part of the mandible, the articulation surface with the quadrate, most of the retroarticular process and is slightly visible in lateral view. The retroarticular process projects posterodorsally. The glenoid fossa and the foramen aerum are not exposed. In lateral view, the articular contacts the surangular ventrolaterally and, in medial view, the angular ventrally.

**Hyoid.** Both hyoids (Fig. 4) are preserved and have a recumbent 'L'-shaped outline with a longer ventral than dorsal branch of the cornu. The dorsal branch is flattened and the ventral one is broadened anteriorly. The lateral part of the ventral branch of the cornu is slightly

bowed medially, whereas its medial part is nearly straight and dorsoventrally oriented. The anterior-most extension is rounded and has a rough surface. Posterior to this surface there are multiple shallow pits of different sizes. The dorsal surface of the ventral cornual branch has a shallow anteroposteriorly oriented groove. The dorsal branch of the cornu is lateromedially flattened with parallel sides. Its dorsal-most part is slightly posteriorly shifted and has a rugose surface.

**Dentition.** The teeth of *M. acutirostris* are circular in cross-section and differ in size. The premaxillary, anterior maxillary (to the 5th tooth position) and anterior dentary teeth (to the 4th tooth position) have multiple dorsoventrally oriented ridges on their lateral and medial surfaces, and sharp but unserrated edges. In the premaxilla, the 4th tooth is the largest one. In the maxilla, the 1st tooth is small and the following teeth are gradually larger until the 5th maxillary tooth, the largest tooth in the tooth row. Posteriorly, the teeth become gradually smaller, but are still much larger overall than the first four maxillary teeth. The posterior-most four teeth are reduced in size and the smallest in the series. In the mandible, the 4th dentary tooth is the largest one in the anterior half of the lower jaw and projects into a notch between the premaxilla and maxilla. The other anterior dentary teeth are small until reaching the presumably 11th or 12th tooth, which is very broad and even slightly larger than the 4th one. Further posteriorly, the teeth seem to get smaller, but due to the occlusion of the jaws this region is not exposed. The dentary teeth are in line with the maxillary tooth row and the teeth are more widely spaced anteriorly, but closer together posteriorly due to their larger size. An enlarged gap can be found between the 7th and 8th maxillary teeth for the enlarged 11th or 12th tooth.

### Postcranial bones

**Axial skeleton.** The vertebral column (Figs 5–8) is nearly complete and in total, the proatlas, seven cervical, 12 dorsal, two sacral and 15 caudal vertebrae are preserved.

**Proatlas.** The proatlas (Fig. 5A–D) is boomerang-shaped with a posterolateral process on each side. The anterior part is slightly offset from the main body without forming a distinct process. The ventral tubercle is not clearly discernible, but based on the general morphology it is relatively large and at least half the width of the dorsal crest. Sagittally, a well-developed median keel is present that has a slightly rounded dorsal surface and slopes strongly posteriorly.

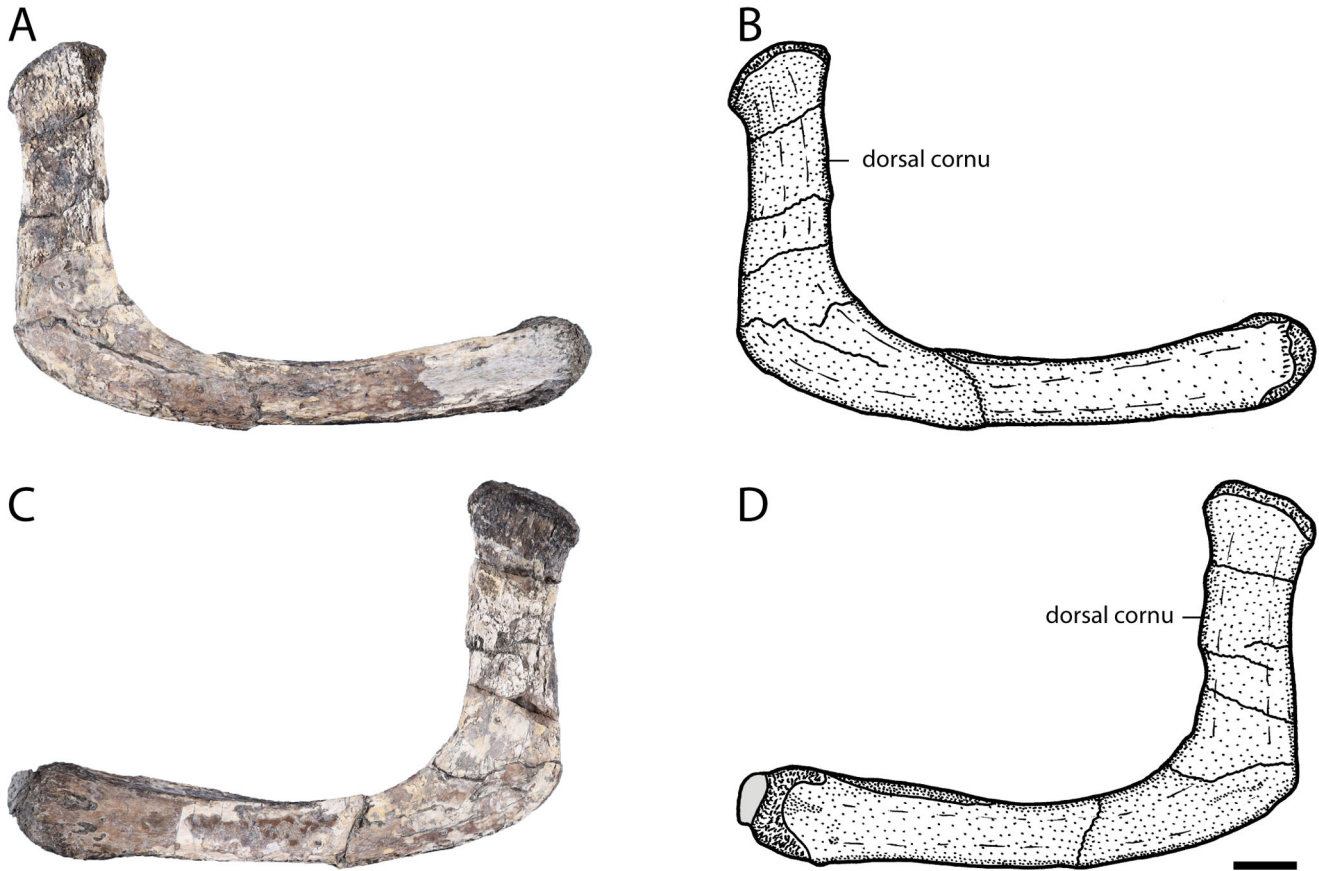
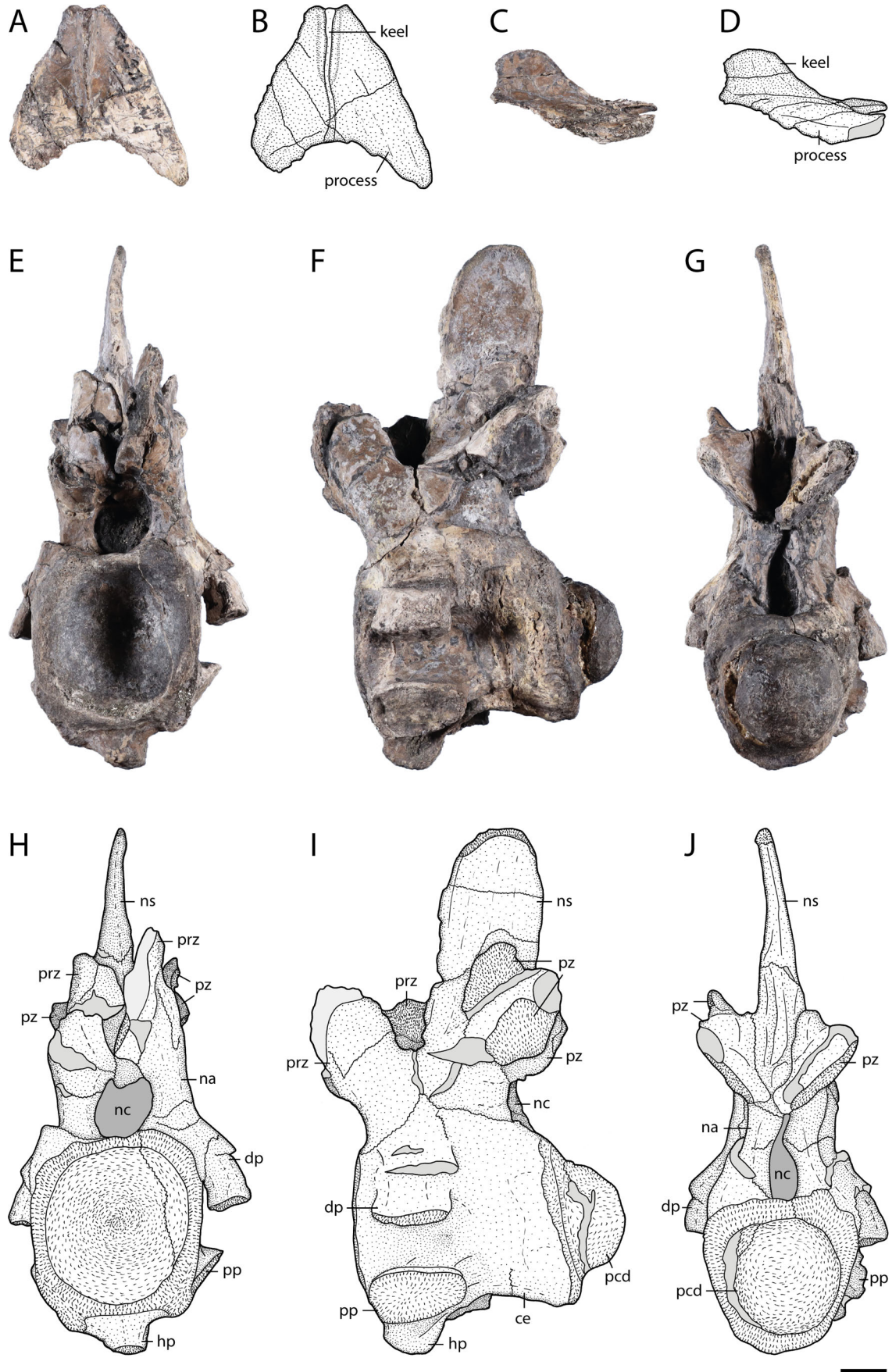


**Figure 4.** *Maomingosuchus acutirostris*, holotype, GPIT-PV-31657, Na Duong Formation, middle to upper Eocene, Vietnam. Right hyoid in **A, B**, lateral and **C, D**, medial views. Scale bar = 1 cm.

**Cervical vertebrae.** The best-preserved cervical vertebra (Fig. 5E–J) is from the anterior region, but its exact position is unknown. Because the cervical vertebrae are rather uniform in morphology, we only describe the best-preserved in detail. The centrum is longer than wide but its height and width are similar. The centrum is constricted between the parapophysis and diapophysis and is ventrally convex in lateral view. The surface is smooth but bears small nutritional foramina below the diapophysis. The anterior articular surface is rounded and slightly more expanded dorsoventrally than the centrum. The posterior condylus is rounded. The hypapophysis is short and does not reach the middle of the centrum. Posteroventrally, a short shallow ridge is discernible. The articular surface of the parapophysis is oval and projects mostly laterally. The slightly damaged diapophysis is lateroventrally oriented and its articular surface is oval and smaller than the articular surface of the parapophysis. The prezygapophysis is oval-shaped and larger than the postzygapophysis. It projects dorsally, whereas the oval-shaped postzygapophysis turns ventrally, both at a 45° angle. The neural spine is nearly

as high as the ventral part of the vertebra, is anteroposteriorly broad and slightly rounded dorsally.

**Dorsal vertebrae.** The best-preserved dorsal vertebra (Fig. 6) is from the anterior region, but its exact position is unknown. Because the dorsal vertebrae, like the cervical vertebrae (see above), are rather uniform in morphology, we only describe the best-preserved dorsal vertebra in detail. The centrum is nearly as long as wide but damaged by deep cracks. The anterior articular surface is round and wider than the centrum, while the posterior condylus seems to be nearly equal in size to the centrum. Ventrally, the centrum is slightly convex in lateral view. Its surface is smooth without visible foramina. The hypapophysis is narrow and anteriorly oriented, and does not reach the central part of the centrum. The transverse process is relatively slender and projects horizontally at an angle of 90° from the centrum. The parapophysis is located anteroventrally at mid-length and the diapophysis is positioned on the distal end of the transverse process. The prezygapophysis projects dorsally and seems to be larger than the



postzygapophysis. The latter faces ventrally with an oval articular surface. A deep groove is present between the postzygapophyses. The neural spine is long and relatively low. Its dorsal tip is generally wide but broader anteriorly than posteriorly.

**Sacral vertebra.** Both sacral vertebrae (Fig. 7) are preserved. In the first sacral vertebra, the lateral extensions of the sacral ribs are covered by osteoderm fragments, the neural spine is broken into two pieces and the neural canal is damaged due to dorsoventral compression. The second sacral vertebra is also covered by osteoderms and its neural spine is broken but the neural canal is intact.

The centrum of the first sacral vertebra (Fig. 7A–F) is nearly as broad as long, and anteriorly and posteriorly slightly ventrally curved and posteriorly sloped. The surface of the centrum is smooth without discernible foramina. On the ventral part of the centrum there is a sulcus reaching from near its posterior end to the middle of the centrum. The anterior articular surface is concave, lateromedially expanded and deep, whereas the posterior articular surface is also expanded but nearly flat with only a very slight concavity. The sacral rib is dorsoventrally compressed. The anterior extension of the articular surface for the ilium reaches further laterally than the posterior one. The prezygapophysis is one-quarter larger than the postzygapophysis and its articular surface is rectangular. The prezygapophysis projects dorsally, whereas the postzygapophysis turns ventrally. The neural spine is long and reaches two-thirds of the dorsoventral length of the centrum. Its dorsal-most extension is damaged but seems to be slightly broader anteriorly than posteriorly.

The second sacral vertebra (Fig. 7G–L) has a similar morphology to the first, but the sacral ribs are anteroposteriorly compressed. The centrum has small nutritional foramina anterolaterally and the sulcus on the ventral surface is less pronounced than in the first sacral. The centrum is nearly straight in lateral view with only a slight ventral projection at its anterior and posterior ends. The anterior articular surface with the first sacral vertebra is wide and flat with a slight concavity. The posterior articular surface is also wide but with a deep concavity for the anterior condylus of the first caudal vertebra. The lateral articular surface of the sacral rib with the ilium is boomerang-shaped with a posterodorsal extension contacting the posterior part of

the iliac blade. The prezygapophysis is larger than the postzygapophysis and projects dorsally, whereas the postzygapophysis turns ventrally, and both have a lateromedially shifted angle of 45°. The neural spine is broken but its height is around two-thirds of the dorsoventral length of the centrum.

**Caudal vertebrae.** The first caudal vertebra (Fig. 8A–F) differs significantly from the more posterior caudal vertebrae and is described separately. The first caudal vertebra is biconvex and its centrum is similar to the centrum of the sacral vertebra in being as wide as it is long. The surface of the centrum is mostly smooth and no sulcus is present, but the ventral part slightly posterior to the anterior condylus has a rugose surface. In lateral view, the centrum is concave with a strong ventral shift posteriorly. Both condyles are similarly sized with the anterior condylus being slightly broader, whereas the posterior condylus is more rounded. The transverse process is incomplete but its lateral-most part shifts slightly posteriorly. The prezygapophysis is larger than the postzygapophysis and its articular surface is oval. The neural spine is elongated but narrower than the neural spines of the sacral vertebrae.

More posteriorly positioned caudal vertebrae (Fig. 8G–L) have a slenderer morphology than the first caudal vertebra and the centrum is elongated, mediolaterally narrow and slightly convex in lateral view. The centrum tapers towards its middle part and a deep sulcus extends over the whole length of the centrum on its ventral surface. The anterior articular surface is rounded and concave, whereas the posterior articular surface has a round condylus. The transverse process is incomplete and projects straight from the centrum at almost 90°. The articular surface of the prezygapophysis is oval and projects dorsally, whereas the articular surface of the postzygapophysis turns ventrally. The neural spine is posteriorly shifted. In the anterior caudal vertebrae, the spine is elongated and flares towards the postzygapophyses. In the posterior caudal vertebrae, the spine tapers into a rod-like morphology and is shifted even more posteriorly and transverse processes are lost.

**Chevron.** The articular surface of the chevron (Fig. 8M–P) for the caudal vertebra is dumbbell-shaped and the haemal canal is rectangular and slightly ventrally tapered. The haemal arch is narrow in anteroposterior view but expanded in lateral view. The haemal spine

←  
**Figure 5.** *Maomingosuchus acutirostris*, holotype, GPIT-PV-31657, Na Duong Formation, middle to upper Eocene, Vietnam. Proatlas in **A, B**, dorsal and **C, D**, lateral left views. Cervical vertebra in **E, H**, anterior, **F, I**, lateral left and **G, J**, posterior views. **Abbreviations:** **ce**, centrum; **dp**, diapophysis; **hp**, hypapophysis; **na**, neural arch; **nc**, neural canal; **ns**, neural spine; **pcd**, posterior condylus; **pp**, parapophysis; **prz**, prezygapophysis; **pz**, postzygapophysis. Scale bar = 1 cm.

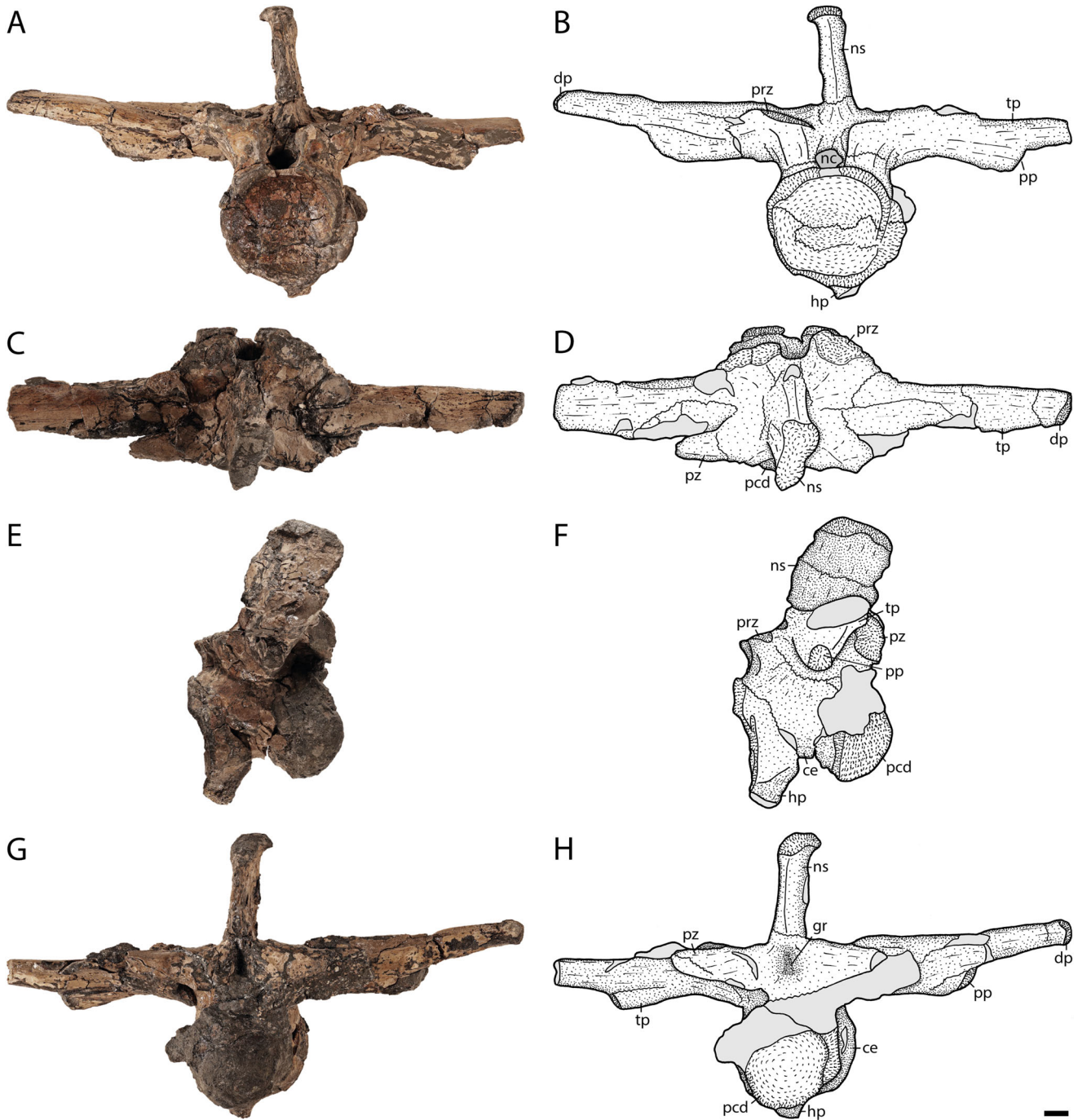


**Figure 6.** *Maomingosuchus acutirostris*, holotype, GPIT-PV-31657, Na Duong Formation, middle to upper Eocene, Vietnam. Dorsal vertebra in **A, B**, anterior, **C, D**, dorsal, **E, F**, lateral and **G, H**, posterior views. **Abbreviations:** **ce**, centrum; **dp**, diapophysis; **gr**, groove; **hp**, hypapophysis; **nc**, neural canal; **ns**, neural spine; **pcd**, posterior condylus; **pp**, parapophysis; **prz**, prezygapophysis; **pz**, postzygapophysis; **tp**, transverse process. Scale bar = 1 cm.

comprises around two-thirds of the total chevron length and is slightly thickened at its ventral-most part.

**Atlantal rib.** The atlantal rib (Fig. 9A–D) is elongated and flat. The articular surface with the atlas is kidney-

shaped and the anterior part of the rib has parallel sides. Neither a large articular facet for the other atlantal rib nor a thin medial lamina are present. The medial part is slightly concave, whereas the lateral part is slightly convex. From the middle part onwards, the rib expands and

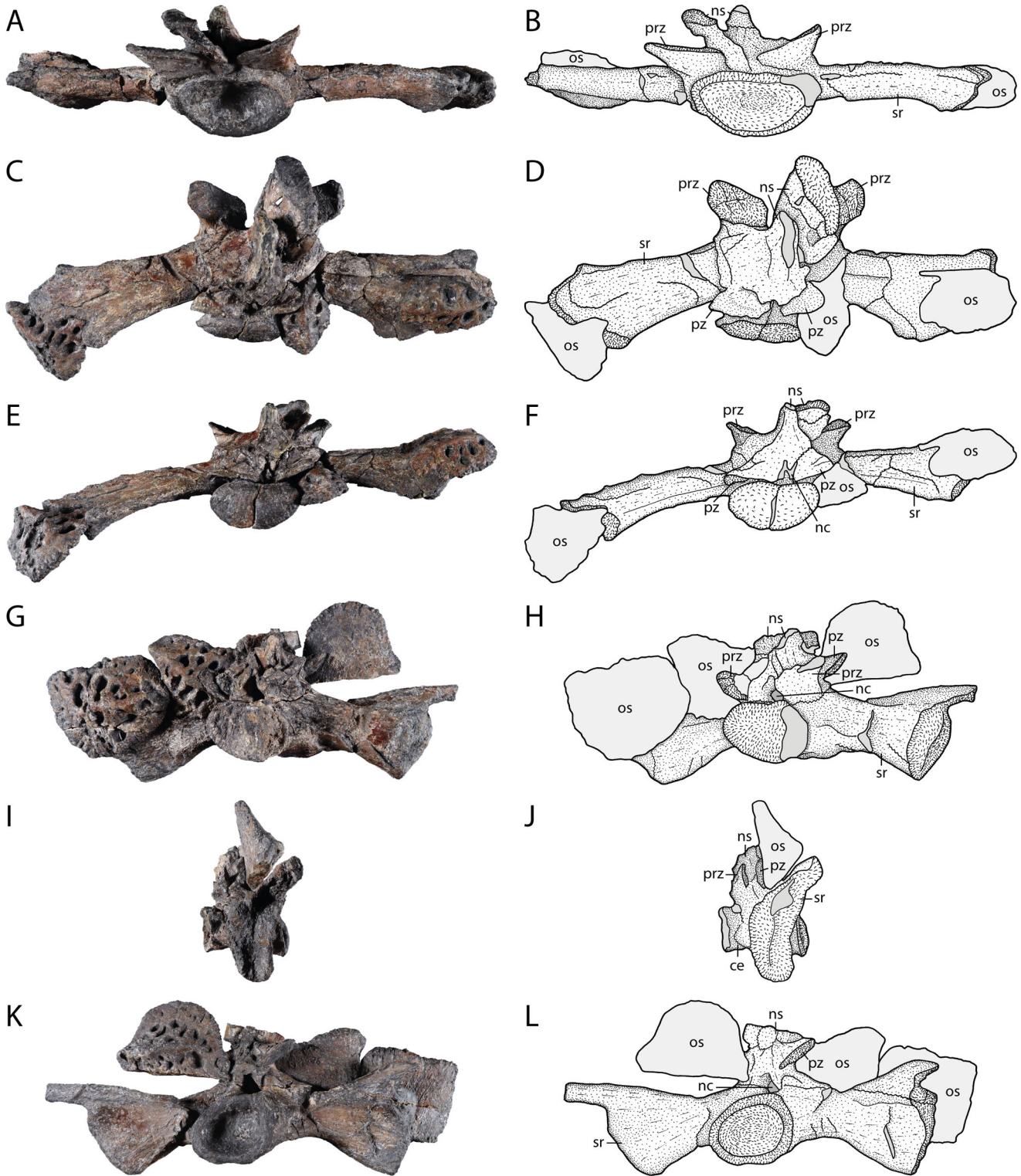


**Figure 7.** *Maomingosuchus acutirostris*, holotype, GPIT-PV-31657, Na Duong Formation, middle to upper Eocene, Vietnam. First sacral vertebra in **A, B**, anterior, **C, D**, dorsal and **E, F**, posterior views. Second sacral vertebra in **G, H**, anterior, **I, J**, lateral left and **K, L**, posterior views. **Abbreviations:** ce, centrum; nc, neural canal; ns, neural spine; os, osteoderm; prz, prezygapophysis; pz, postzygapophysis; sr, sacral rib. Scale bar = 1 cm.

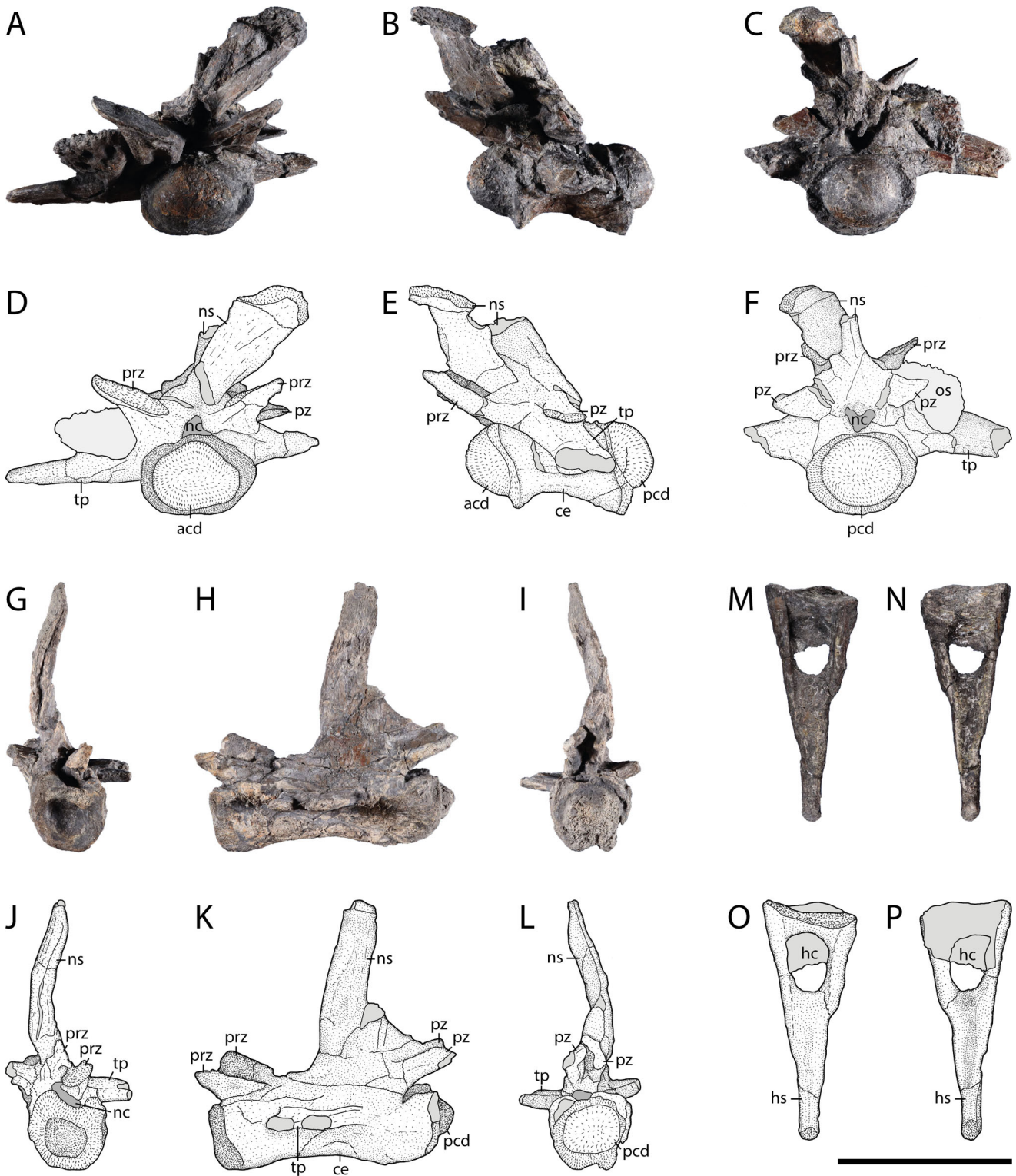


**Figure 8.** *Maomingosuchus acutirostris*, holotype, GPIT-PV-31657, Na Duong Formation, middle to upper Eocene, Vietnam. First caudal vertebra in **A, D**, anterior, **B, E**, lateral and **C, F**, posterior views. Middle caudal vertebra in **G, J**, anterior, **H, K**, lateral left and **I, L**, posterior views. Chevron in **M, O**, anterior and **N, P**, posterior views. **Abbreviations:** **acd**, anterior condylus; **ce**, centrum; **hc**: haemal canal; **hs**, haemal spine; **nc**, neural canal; **ns**, neural spine; **os**, osteoderm; **pcd**, posterior condylus; **prz**, prezygapophysis; **pz**, postzygapophysis; **tp**, transverse process. Scale bar = 1 cm.

forms a dorsal process, which tapers rapidly posteriorly. The ventral part expands only slightly before projecting straight posteriorly.

**Cervical ribs.** The best-preserved cervical rib is from the anterior region (Fig. 9E–J), but its exact position is unclear. The dorsal part consists of two columnar processes, the medial capitulum and the lateral tuberculum. The capitulum contacts the parapophysis of the cervical vertebra, whereas the tuberculum contacts the diapophysis. The capitulum is shorter than the tuberculum, but its articular surface is broader and rounded, while that of the tuberculum is more elongate. The anterior region of the ventral part of the bone is shorter than the posterior extension and steep, whereas the posterior part is flat with a deep medial concavity.

A posterior left cervical rib (Fig. 9K–N) is preserved and likely contacted the 6th cervical vertebra. The capitulum is elongated and much longer than the tuberculum. The articular surface of the capitulum is small and rounded, while that of the tuberculum is nearly double the size and broad. A lateral projecting lamina was folded due to compression, but would normally project perpendicular to the shaft. The posteroventrally projecting shaft tapers slightly distally and has a lateral ridge contacting the lamina and reaches the posterior third of the bone. The medial part of the shaft is flat.

**Dorsal rib.** The dorsal ribs are incomplete, but their general morphology does not seem to differ from other tomistomines.

**Scapula.** Both scapulae (Fig. 10A, B, E, F) are present, but only the right one is well preserved. The scapular blade expands dorsally, with a relatively straight anterior edge. The deltoid crest is partially covered by a dorsal rib, but the bulge of the crest is relatively narrow. The articular surface for the coracoid is elongate, but lateromedially flattened due to compression. Anterior to the deltoid crest and anterodorsal to the articulation surface, the scapula is elongated and rectangular. The glenoid fossa is ventrolaterally oriented and oval.

**Coracoid.** The left coracoid (Fig. 10C, D, G, H) is better-preserved, but lateromedially compressed. The shaft is slightly bowed and the coracoid blade expands ventrally, but is narrow compared to the scapular blade. Anteroventrally, the blade has a small process projecting anteriorly. The articular surface for the scapula is elongate, but lateromedially flattened due to compression. Anterior to the articular surface with the scapula, the coracoid is elongated and rectangular. The glenoid fossa has an oval outline and the coracoid foramen is small and situated well anterior to the glenoid fossa.

**Humerus.** The right humerus (Fig. 11A–H) is better preserved than the left. The bone is relatively slender and its surface is mostly smooth with rugose areas ventral to the proximal and dorsal to the distal articulation surfaces. The humeral head is divided in an anterior and a posterior tubercle. The anterior tubercle forms the proximal-most point of the humerus, whereas the posterior tubercle is posterodistally shifted. The deltopectoral crest has a concave surface and projects nearly perpendicular to the shaft. Close to its distal end, the humerus has a visible central concavity on its dorsal and ventral part. Distally, the medial and lateral condyles form the articular surfaces for the radius and ulna. Both condyles are rounded with the lateral condylus being slightly larger. Scars for the musculature are not visible.

**Ulna.** Only the left ulna (Fig. 11I–L) is preserved. It is sigmoidal and proximally expanded. The articular surfaces are compressed. The small olecranon process forms its proximal-most point and the proximal articular surface slopes anteriorly. The distal articular surface is kidney-shaped.

**Ilium.** The right ilium (Fig. 12A–D) is better preserved, but deformed with its posterodorsal end shifted, whereas the left ilium is less deformed but fused to the left ischium. The dorsal part of the bone has a rugose surface, is slightly sigmoidal with a shallow indentation posteriorly and a small anterior process. The iliac blade in general is narrow but posteroventrally slightly broadened. In medial view, the bone has two prominent scars for articulation with the first and second sacral ribs. The anterior scar is oval, whereas the posterior scar is elongated and reaches the ventral part of the iliac blade. In lateral view, the supraacetabular crest is narrow with a rounded outline and the acetabulum forms a broadly rounded depression. The ventral part of the ilium forms the articular surfaces for the ischium. The posterior articular surface is boomerang-shaped, whereas the anterior one is elongate and kidney-shaped. The acetabulum foramen is visible between the two surfaces.

**Ischium.** The right ischium (Fig. 12E–H) is better preserved, but has a deformed posteroventral part, whereas the left ischium is less deformed but fused to the left ilium. The ventral part is formed by the ventromedially bowed ischium blade and the anteroventral part of the blade is nearly rectangular, whereas the posterior part extends far posteriorly. The dorsal part of the bone can be divided into two processes. The posterior process forms the articular surface with the posterior part of the ilium. This surface is triangular with a small elongate anterior process. The anterior process is slenderer and has two separated articular surfaces. The dorsal one contacts the anterior articular surface of the ilium, whereas



**Figure 9.** *Maomingosuchus acutirostris*, holotype, GPIT-PV-31657, Na Duong Formation, middle to upper Eocene, Vietnam. Left atlantal rib in **A, B**, lateral and **C, D**, medial views. Right anterior cervical rib in **E, H**, dorsal, **F, I**, medial and **G, J**, lateral views. Left posterior cervical rib in **K, L**, lateral and **M, N**, medial views. **Abbreviations:** ca, capitulum; tu, tuberculum. Scale bar = 1 cm.

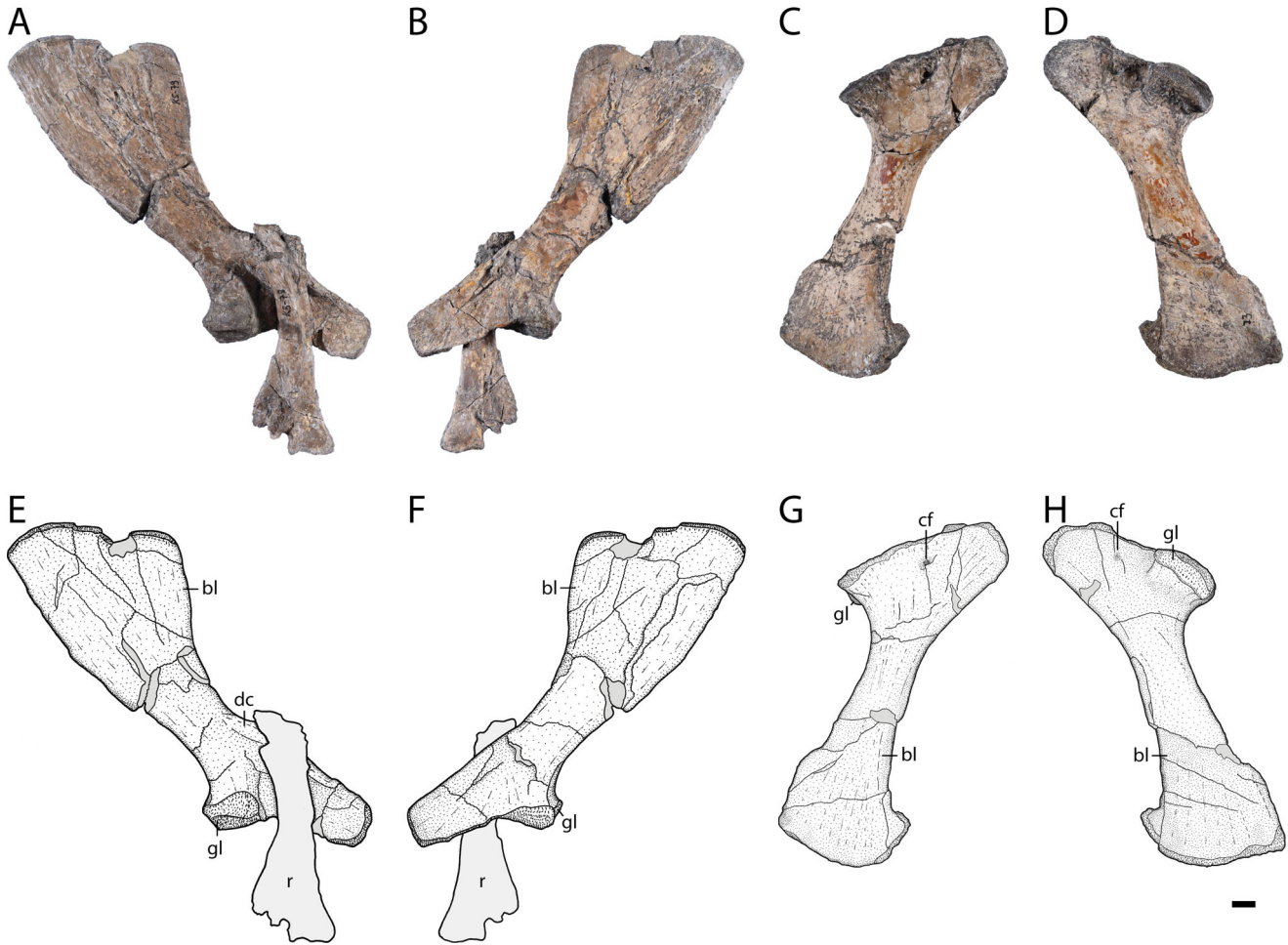


**Figure 10.** *Maomingosuchus acutirostris*, holotype, GPIT-PV-31657, Na Duong Formation, middle to upper Eocene, Vietnam. Right scapula in **A**, **E**, lateral and **B**, **F**, medial views. Right coracoid in **C**, **G**, lateral and **D**, **H**, medial views. **Abbreviations:** **bl**, blade; **cf**, coracoid foramen; **dc**, deltoid crest; **gl**, glenoid, **r**, rib. Scale bar = 1 cm.

the anteroventrally projecting one contacts the pubis. The articular surface with the ilium is lateromedially elongate and the articular surface with the pubis is oval. Between the anterior and posterior process, the acetabulum foramen is present.

**Pubis.** The left pubis (Fig. 12I–L) is well-preserved. Its ventral blade flares nearly symmetrically with a rounded ventral edge. The posteroventral part of this edge is vertical for a short distance. The blade is lateromedially flattened and the shaft is oval in cross-section. The dorsal articular surface is oval and slightly shifted posteriorly. It contacts the anteroventral articular surface of the anterior process of the ischium.

**Femur.** The left femur (Fig. 13A–H) is better preserved, relatively slender, larger than the humerus and has a sigmoidal outline with a slight torsion. The femoral head is compressed and therefore appears to be oval. Directly ventral to the femoral head, the bone surface is rugose,

with small openings, most likely representing nutritional foramina. Proximocaudally, the insertion scar for the *M. puboischiofemoralis externus* is visible. The 4th trochanter is prominent and positioned on the proximal one-third of the bone. The distal end of the femur is divided into two condyles: a lateral condylus and a slightly smaller medial condylus. In dorsal view, a small groove between the two condyles is present, whereas a deeper depression can be seen in ventral view.

**Tibia.** The left tibia (Fig. 13I–L) is poorly preserved and its shaft is damaged. The proximal part is divided into a medial and lateral condylus. The medial condylus is oval and separated from the larger lateral one by a groove. The distal articular surface is crescent-shaped with an anterior and a posterior condylus, which are separated from each other by a shallow groove.

**Fibula.** The left fibula (Fig. 13M–P) is poorly preserved, with a proximal articular surface that has been



**Figure 11.** *Maomingosuchus acutirostris*, holotype, GPIT-PV-31657, Na Duong Formation, middle to upper Eocene, Vietnam. Left humerus in **A, B**, dorsal, **C, D**, ventral, **E, G**, proximal and **F, H**, distal views. Left ulna in **I, J**, lateral and **K, L**, medial views. **Abbreviations:** **acd**, anterior condylus; **atb**, anterior tubercle; **dpc**, deltopectoral crest; **hh**, humeral head; **lcd**, lateral condylus; **mcd**, medial condylus; **op**, olecranon process; **pcd**, posterior condylus; **ptb**; posterior tubercle. Scale bar = 5 cm.

nearly completely lost. The shaft is oval in cross-section. The distal articular surface is bean-shaped and slightly shifted posteriorly.

**Metatarsals.** The left metatarsal II (Fig. 13Q–T) is the best preserved and its proximal articular surface is flat and elongate. The shaft is flattened proximally, but is slightly oval in cross-section distally. The distal articular surface is broad with a nearly rectangular outline. The two condyles

are very low with only a very shallow groove separating them. In ventral view, a deep depression is visible directly proximal to the distal articular surface.

**Osteoderms.** Several dorsal osteoderms (Fig. 14A, B), some putative lateral osteoderms (Fig. 14C, D) and many osteoderm fragments are preserved – most of them occurring isolated. The osteoderm central surface is strongly ornamented with a pattern of deep oval and

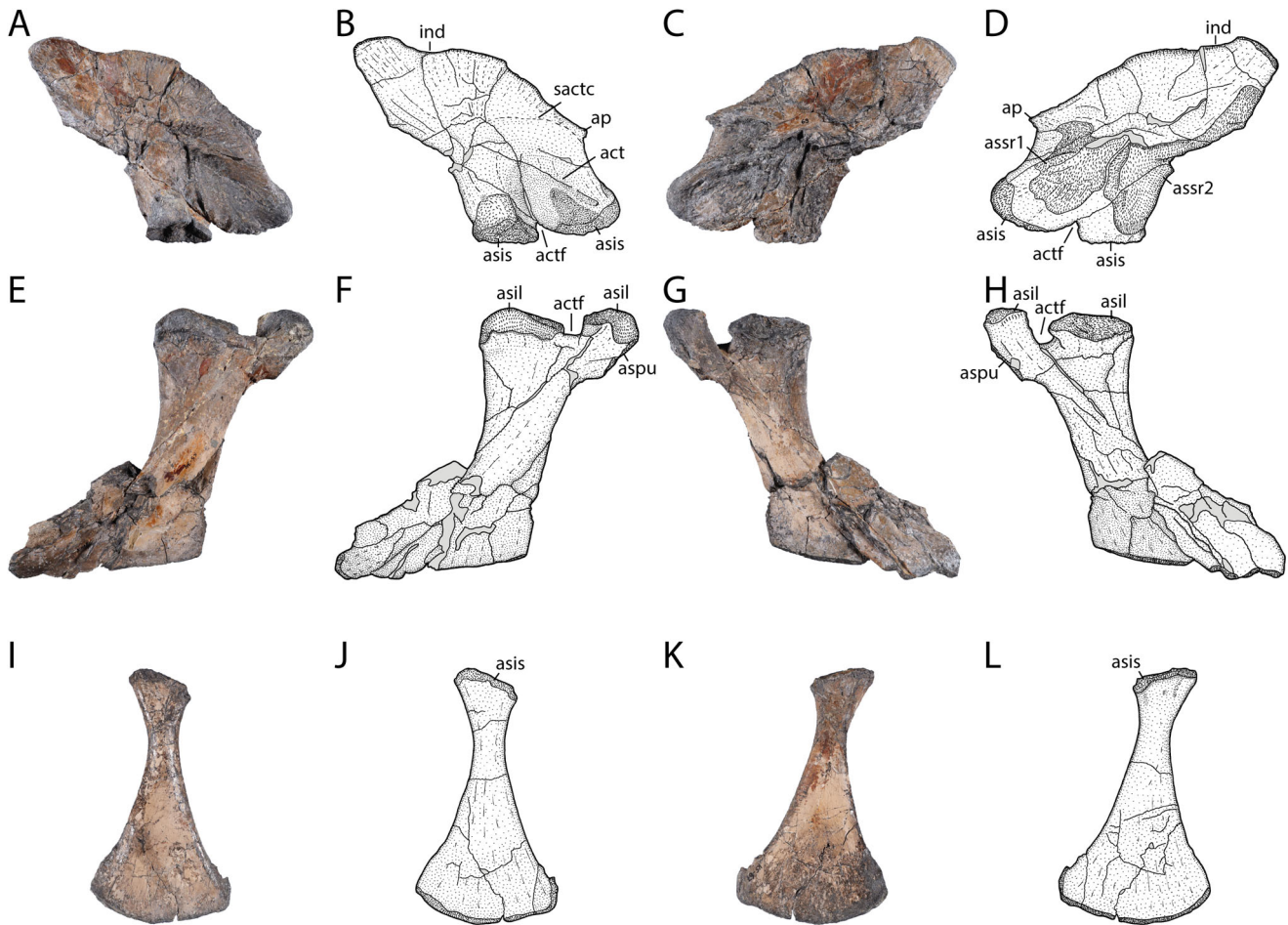


**Figure 12.** *Maomingosuchus acutirostris*, holotype, GPIT-PV-31657, Na Duong Formation, middle to upper Eocene, Vietnam. Right ilium in **A, B**, lateral and **C, D**, medial views. Right ischium in **E, F**, lateral and **G, H**, medial views. Left pubis in **I, J**, lateral and **K, L**, medial views. **Abbreviations:** **act**, acetabulum; **actf**, acetabulum foramen; **ap**, anterior process; **asil**, articulation surface with ilium; **asis**, articulation surface with ischium; **aspu**, articulation surface with pubis; **assr1**, articulation surface with sacral rib 1; **assr2**, articulation surface with sacral rib 2; **ind**, indentation; **sactc**, supraacetabular crest. Scale bar = 1 cm.

round pits. Towards the edges, the surface is smooth. The dorsal osteoderms are rectangular with a broad facet to contact the anteriorly positioned osteoderm. A well-developed dorsal keel is present, projecting from slightly posterior of the anterior facet to the posterior end of the osteoderm. The putative lateral osteoderms have a more oval outline and are slightly curved, but show a well-developed dorsal keel also. A contact surface is not visible but the edges seem to be damaged.

## Comparisons

### Comparisons with other *Maomingosuchus* specimens

**Skulls.** *Maomingosuchus acutirostris*, *Maomingosuchus petrolicus* and the Krabi-*Maomingosuchus* are all

medium-sized tomistomines with skull lengths of slightly over 500 mm (*M. acutirostris*, 546 mm; *M. petrolicus*, 280–503 mm, with NMNS005825-F044383 slightly larger based on the incomplete skull table [see Shan *et al.* 2017]; Krabi-*Maomingosuchus*, >500 mm, anterior part missing [see Martin *et al.* 2019]). The snout length is also very similar within *Maomingosuchus* with a snout-to-skull length ratio ranging between 0.71 and 0.72, but the snout shape differs slightly: in *M. petrolicus* and Krabi-*Maomingosuchus* it is narrow, with only a slight broadening at the level of the 5th maxillary tooth, while the snout of *M. acutirostris* is much broader at this level with a strongly enlarged 5th maxillary tooth.

**Cranial openings.** The general skull shape, as well as the cranial openings, are very similar in all *Maomingosuchus* specimens. The external nares of both



*M. acutirostris* and *M. petrolicus* are large and broader anteriorly than posteriorly (unknown in the Krabi specimen), but the premaxillary process reaching into the external naris described for *M. petrolicus* (Shan *et al.* 2017, p. 675), is not visible in *M. acutirostris*. The orbit of *M. acutirostris* is more elongated than the rounded one of *M. petrolicus* whereas the supratemporal fenestra is smaller than in the latter, resulting in a different ratio of the supratemporal fenestral length to orbit length (0.57 in *M. acutirostris*; 0.83 in *M. petrolicus*; and 0.76 for Krabi-*Maomingosuchus*).

The supratemporal bar in *M. petrolicus* is thin compared to skull table width (Shan *et al.* 2017, fig. 2). Its ratio is only around 0.07, while it is 0.11 in *M. acutirostris*. In Krabi-*Maomingosuchus* this ratio is difficult to determine, but the bar seems to be relatively broad (Martin *et al.* 2019, fig. 1), and the ratio appears to be closer to the ratio seen in *M. acutirostris*.

**Skull bones.** In general, the shapes of the individual skull bones and their sutures are similar in all *Maomingosuchus* specimens.

The premaxilla is only known for *M. acutirostris* and *M. petrolicus*, but in both species the anterior-most part differs, with a short and rounded anterior snout in *M. petrolicus* (Shan *et al.* 2017, figs 2, 4) and an elongated and acute one in *M. acutirostris*.

The anterior part of the prefrontal lies at the same level as the anterior part of the frontal in *M. acutirostris* and Krabi-*Maomingosuchus*. According to Shan *et al.* (2017), this condition is variable in *M. petrolicus*, as in some specimen (e.g. NMNS005146-F041793) the frontal is shorter than the prefrontal.

In *M. petrolicus* and Krabi-*Maomingosuchus* the prefrontal slightly overhangs the orbital margin (Martin *et al.* 2019). This is not the case in *M. acutirostris* but this could be a compressional artefact.

The supraoccipital is largely exposed on the skull table in *M. acutirostris* and *M. petrolicus*. In *M. petrolicus*, the exposure and shape of the supraoccipital is variable and either more rectangular, as in DM-F0001, or more triangular, as in NMNS002060-F027511 (Shan *et al.* 2017, fig. 3). In *M. acutirostris*, it is more triangular, whereas in Krabi-*Maomingosuchus* the condition is unknown.

Krabi-*Maomingosuchus* differs from *M. acutirostris* and *M. petrolicus* in the position of the

surangular–dentary suture in the external mandibular fenestra. Only in Krabi-*Maomingosuchus* does the suture reach the posterior-most corner (Martin *et al.* 2019, fig. 2), whereas the suture intersects the fenestra anterior to its posterior margin in *M. acutirostris* and *M. petrolicus*.

**Teeth.** In general, the tooth rows and teeth of *Maomingosuchus* specimens are similar but there are some noteworthy differences. In total, there are 15 maxillary teeth in *M. acutirostris* and *M. petrolicus*. In Krabi-*Maomingosuchus* the tooth number is difficult to assess, but at least 14 maxillary alveoli are visible (Martin *et al.* 2019, fig. 1). The 1st dentary tooth perforates the premaxilla anterior to the external naris in *M. acutirostris* and *M. petrolicus*, which is a rare character among tomistomines (see below). Due to the missing tip of the snout this condition is unknown in Krabi-*Maomingosuchus*. In *Maomingosuchus*, the premaxillary, anterior maxillary and anterior dentary teeth have clearly visible dorsoventrally projecting ridges on their lateral and mesial surfaces and the teeth have sharp outer edges (Shan *et al.* 2017, fig. 4; Martin *et al.* 2019, fig. 3).

Differences between the *Maomingosuchus* specimens occur in tooth size. In *M. acutirostris*, the 5th maxillary tooth and the 11th or 12th dentary tooth are enlarged, whereas in *M. petrolicus* (Shan *et al.* 2017, fig. 2) and Krabi-*Maomingosuchus* (Martin *et al.* 2019, fig. 1), the 5th maxillary tooth is also enlarged but smaller overall. In *M. acutirostris* and *M. petrolicus* the anterior alveoli increase in size towards the 5th maxillary tooth, whereas there is no size difference in Krabi-*Maomingosuchus*, with the 5th maxillary tooth being only slightly larger (Martin *et al.* 2019, fig. 1).

The spacing of the teeth posterior to the 5th maxillary alveolus also differs within *Maomingosuchus*. A wider distance between the 7th and 8th maxillary alveoli for the enlarged 11th or 12th dentary tooth is only present in *M. acutirostris* and to a smaller degree in *M. petrolicus* (Shan *et al.* 2017, fig. 4c, e). In Krabi-*Maomingosuchus* there are no enlarged dentary teeth and therefore no enlarged maxillary distance is present (Martin *et al.* 2019, fig. 2).

**Postcranial skeleton.** Two differences between *M. acutirostris* and *M. petrolicus* are present in the postcranial skeleton but not preserved for Krabi-*Maomingosuchus*. On the atlantal rib, there is a process on the dorsal

←  
**Figure 13.** *Maomingosuchus acutirostris*, holotype, GPIT-PV-31657, Na Duong Formation, middle to upper Eocene, Vietnam. Left femur in **A, B**, dorsal, **C, D**, ventral, **E, G**, proximal and **F, H**, distal views. Left tibia in **I, J**, anterior and **K, L**, posterior views. Left fibula in **M, N**, lateral and **O, P**, medial views. Left metatarsal two in **Q, R**, dorsal and **S, T**, ventral views. **Abbreviations:** **4th tr**, fourth trochanter; **acd**, anterior condylus; **fh**, femur head; **lcd**, lateral condylus; **mcd**, medial condylus; **mpe**, insertion scar for the *M. puboischiofemoralis externus*; **pcd**, posterior condylus. Scale bar = 5 cm.

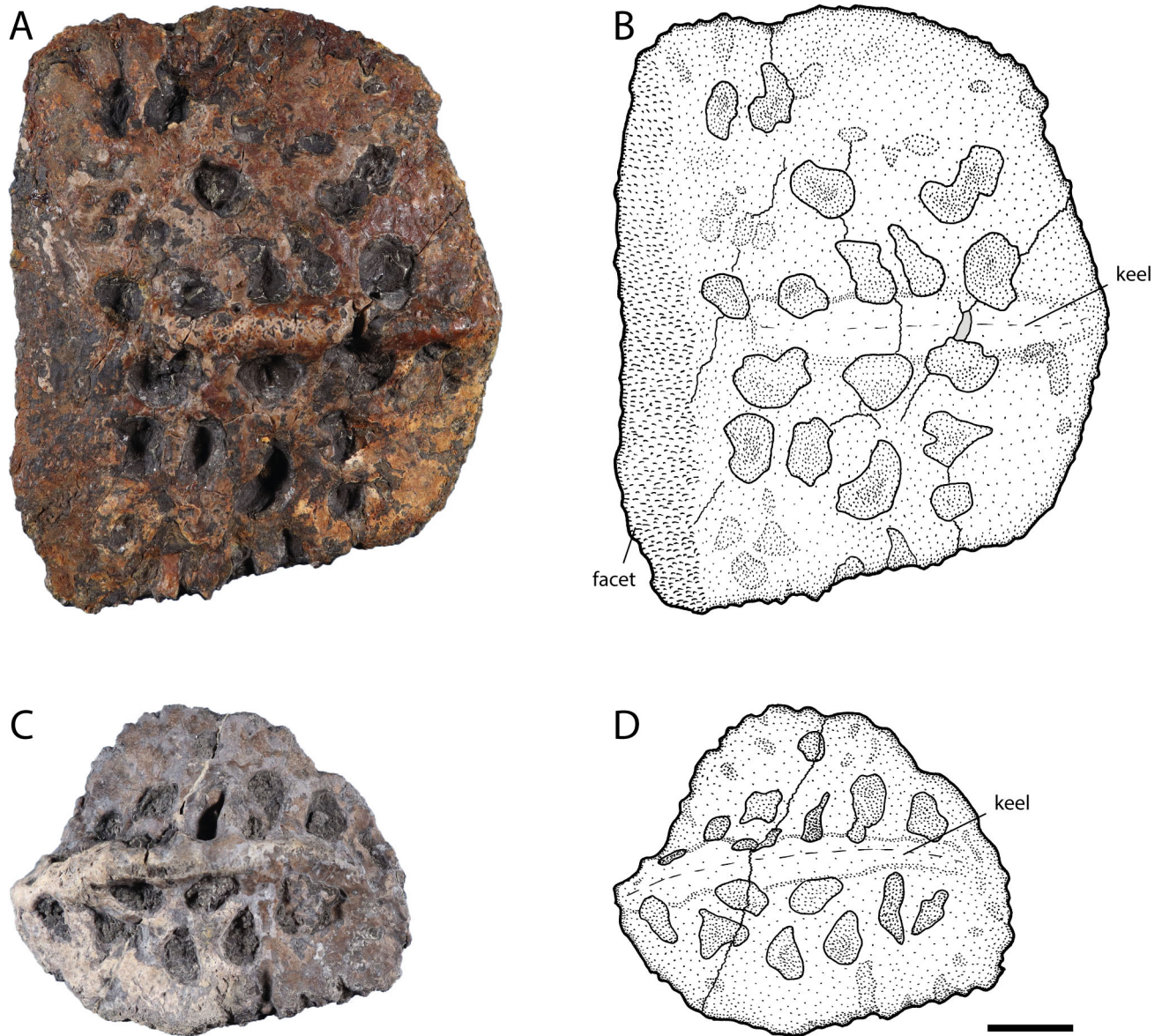


**Figure 14.** *Maomingosuchus acutirostris*, holotype, GPIT-PV-31657, Na Duong Formation, middle to upper Eocene, Vietnam. Dorsal midline osteoderm in **A, B**, dorsal view. Presumably lateral osteoderm in **C, D**, dorsal view. Scale bar = 1 cm.

margin in *M. acutirostris*, while this region seems to be smooth in *M. petolicus* (described as similar to *T. schlegelii* by Shan *et al.* [2017]). The ilium of *M. acutirostris* has a prominent anterior process. This region is poorly preserved in *M. petolicus* (Shan *et al.* 2017, fig. 10), but the anterior iliac border does not seem to lead into a process comparable to the one in *M. acutirostris*.

#### Comparisons with other taxa

**Skulls.** *Maomingosuchus* is a medium-sized tomistomine genus with a skull reaching slightly more than 500 mm

(see above). Tomistomines in general have a broad size range, from around 430 mm in *Kentisuchus spenceri* and *Dollosuchooides* to over 1 m in the giant species *Toyotamaphimeia*. The extant *Tomistoma schlegelii* exhibits remarkable size variation with a typical skull length of around 500 mm to a maximum of over 800 mm (Whitaker & Whitaker 2008). By contrast, the skull to snout ratio in Tomistominae remains relatively constant and ranges from around 0.7 to 0.8. With a skull to snout ratio between 0.71 and 0.72, *Maomingosuchus* is one of the shortest-snouted taxa, comparable to *Maroccosuchus* and *K. spenceri*. This is shorter than

extant *T. schlegelii* (with a ratio of 0.74) and much shorter than long snouted Miocene taxa like *Gavialosuchus* (with a ratio of 0.79).

Snout shape differs among tomistomines. In *Maroccosuchus*, the snout is laterally broadened at the level of the 5th maxillary tooth (Jouve *et al.* 2015, figs 3, 8), which is also the case in *Megadontosuchus* (Piras *et al.* 2007, fig. 1) and *M. acutirostris*, but to a slightly lesser degree. On the other hand, almost no expansion is present in *T. schlegelii*, ‘*Tomistoma*’ *calaritanum* Capellini, 1890 (Nicholl *et al.* 2020, fig. 10), *Dollosuchoides* (Brochu 2007, fig. 3) and *Gavialosuchus* (Toula & Kali 1885, table 1). Most other tomistomines have a slight expansion of the snout at the level of their largest maxillary tooth.

**Cranial openings.** The external naris in all known *Maomingosuchus* specimens with a preserved snout is large and anteriorly wider than posteriorly, with a nearly straight lateromedially projecting anterior margin, which is unique among tomistomines. In species like *T. schlegelii* or *Melitosaurus champsoides* Owen, 1849 (Nicholl *et al.* 2020, fig. 2) the external naris is smaller and oval. In species like *K. spenceri* (Brochu 2007, fig. 2), the external naris is relatively large and oval. A more rectangular shape with a straighter anterior margin similar to *Maomingosuchus* can be seen in *Maroccosuchus* (Jouve *et al.* 2015, figs 3, 7) and *Dollosuchoides* (Brochu 2007, fig. 3).

While the difference in orbit size seems to be small among tomistomines, the differences in supratemporal fenestra size are significant. For a longirostrine taxon, *Maomingosuchus* has relatively small fenestrae with broad posterior and lateral margins. Similar small fenestrae are present only in *Paratomistoma* (Brochu & Gingerich 2000, fig. 2). In *T. schlegelii*, *Maroccosuchus*, *Megadontosuchus*, *K. spenceri*, *Thecachampsa carolinensis* (Erickson & Sawyer, 1996), ‘*Tomistoma*’ *cairensis*, ‘*Tomistoma*’ *gaudense* (Hulke, 1871) and ‘*Tomistoma*’ *lusitanica* Antunes, 1961, the supratemporal fenestrae are medium-sized to large, while they are very enlarged in *Dollosuchoides*, *Thecachampsa antiqua* (Leidy, 1852), *Toyotamaphimeia* and *Gavialosuchus*.

The size of the supratemporal fenestrae also affects the shape of the interfenestral bar, which is usually wider in taxa with smaller fenestrae. The broadest bar is found in *Paratomistoma* (Brochu & Gingerich 2000, fig. 2) which also has the smallest fenestrae. The interfenestral bar is relatively broad in *Maroccosuchus* despite its medium-sized fenestrae (Jouve *et al.* 2015, figs 3, 8, 11).

The external mandibular fenestra of *Maomingosuchus* is medium- to large-sized for a tomistomine. In *T.*

*schlegelii* the fenestra is slightly larger, while it is smaller in *Toyotamaphimeia* (Kobayashi *et al.* 2006, figs 11, 12) and *Paratomistoma* (Brochu & Gingerich 2000, fig. 4).

**Skull bones.** In many tomistomines, the anterior-most part of the snout is more elongated, often including a lateral notch for the 1st dentary tooth (e.g. *Melitosaurus*, Nicholl *et al.* 2020, fig. 2; *Dollosuchoides*, Brochu 2007, fig. 3; most *T. schlegelii*). In other taxa, the snout is more rounded (e.g. *Toyotamaphimeia*, Kobayashi *et al.* 2006, fig. 7; *Maroccosuchus*, Jouve *et al.* 2015, figs 3, 7, 8; and *K. spenceri*, Brochu 2007, fig. 2). In *Maomingosuchus petrolicus*, the anterior region is especially short, shorter than in other tomistomines. In some more round-snouted taxa, a perforation of the premaxilla by the first dentary tooth occurs (*Toyotamaphimeia*, Kobayashi *et al.* 2006, figs 7, 15; *K. spenceri*, Brochu 2007, fig. 2; and *M. petrolicus* see above), but for taxa with a more elongated anterior snout this is only the case in *M. acutirostris*.

In *M. petrolicus* and *Krabi-Maomingosuchus*, the prefrontal slightly overhangs the orbit (see above). This is also known for *Maroccosuchus* (Jouve *et al.* 2015, fig. 9), *Penghusuchus* (Shan *et al.* 2009, fig. 2) and *T. schlegelii*. A frontal fossa is only present in *Maomingosuchus*. A similar structure is found in the crocodyloid ‘*Crocodylus*’ *affinis* (Mook 1921, pl. XVI) and *Prodiplacynodon langi* Mook (1941, fig. 2), a narrow ‘U’-shaped structure in the alligatoroid *Bottosaurus harlani* Meyer, 1832 (Cossette & Brochu 2018, figs 4, 5) and a broad ‘U’-shaped structure further anteriorly in the basal eusuchian *Acynodon iberoccitanus* Buscalioni, Ortega & Vasse, 1997 (Martin 2007, fig. 1).

The frontal in *Maomingosuchus* is wide and flat between the orbits, and the edges are not upturned, which is otherwise only known for *Dollosuchoides*. The postorbital bar in *Maomingosuchus* is anteroposteriorly expanded, whereas in most tomistomines the bar is massive but slenderer (e.g. *T. schlegelii*). Otherwise, a broad bar is only found in some basal eusuchians and gharials. The supraoccipital is only slightly exposed on the skull table and barely visible in most tomistomines, but this is pronounced in *Maomingosuchus*, ‘*T.*’ *cairensis* and ‘*Tomistoma*’ *coppensi* Pickford, 1994.

In *Maomingosuchus*, there is a ventrally projecting lamina on the exoccipital covering the entrance to the cranio-quadrangle passage. The character is otherwise only known for basal eusuchians like *Allodaposuchus precedens* Nopcsa, 1928 (Delfino *et al.* 2008, fig. 3) or *Hylaeochampsa vectiana* Owen, 1874 (Clark & Norell 1992, fig. 8) and among crocodylians only for gharials and thoracosaurus. A similar structure is present in

*Penghusuchus*, but here the lamina is more medially oriented.

In *Maomingosuchus acutirostris* and *M. petrolicus*, the surangular–dentary suture intersects the external mandibular fenestra anterior to its posterior border, whereas in *Krabi-Maomingosuchus*, the suture reaches the posterior-most corner of the fenestra (see above). The condition in *Krabi-Maomingosuchus* is unknown in any other tomistomine, but present in some alligatoroids like *Stangerochampsia mccabei* Wu, Brinkman & Russell, 1996, fig. 2, *Navajosuchus mooki* (Simpson, 1930) (Lucas & Estep 2000, fig. 4) or *Orientalosuchus naduogensis* (Massonne *et al.* 2019, fig. 9).

**Teeth.** The total tooth count in tomistomines is variable between species. *Marccosuchus*, *Thecachampsia carolinensis* and ‘*T.*’ *gaudense* have 14 teeth in the maxilla, *Dollosuchoides* and *Maomingosuchus* have a maximum of 15 teeth, *T. schlegelii* and *Toyotamaphimeia* have 16 and *Penghusuchus* 17 teeth.

In *Maomingosuchus*, the 1st dentary tooth perforates the premaxilla anterior to the external naris. In tomistomines, this is only known for *K. spenceri* (Brochu 2007, fig. 2) and some specimens of *T. schlegelii* (C. Brochu, pers. comm.). In *Toyotamaphimeia*, the premaxilla is also perforated by the 1st dentary tooth, but the openings are situated inside the external naris (Kobayashi *et al.* 2006, figs 7, 15). In other taxa, such as *Dollosuchoides* (Brochu 2007, fig. 3) or most *T. schlegelii*, the 1st dentary tooth projects into an anterolateral notch of the premaxilla. In *Marccosuchus*, there is no lateral notch or perforation for the 1st dentary tooth visible in dorsal view (Jouve *et al.* 2015, figs 7, 8), implying that the 1st dentary tooth is small. A perforated premaxilla is rare among tomistomines, but frequently present in members of Crocodylinae, such as *Crocodylus niloticus* Laurenti, 1768, in which the perforations are positioned further anteriorly.

Only the premaxillary, anterior maxillary and anterior dentary teeth of *Maomingosuchus* show dorsoventrally running ridges on their lateral and mesial surface, with sharp outer edges. Strong ridges are found in a tomistomine from the middle Eocene Ikovo locality (Kuzmin & Zvonok 2021, fig. 3) and in non-tomistomines such as *Allodaposuchus precedens* (Martin *et al.* 2016, fig. 11), *Krabisuchus siamogallicus* Martin & Lauprasert, 2010, fig. 5 and *Orientalosuchus naduogensis* (Massonne *et al.* 2019, fig. 10). Fine ridges are known for other tomistomines (such as *T. schlegelii* and *Melitosaurus*). Sharp outer edges on the teeth are present in *Thecachampsia antiqua* (Myrick 2001, fig. 5) and *Marccosuchus* (Jouve *et al.* 2015, p. 15), whereas in other species like *T. schlegelii* and *Melitosaurus*

(Nicholl *et al.* 2020 fig. 3) the teeth are more rounded with shallower edges.

In *M. acutirostris*, the difference in tooth sizes resembles the condition found in *Marccosuchus*, but the gaps between the teeth are distinctly smaller and the dentary is only slightly bent in lateral view, but more curved in *Marccosuchus* (Jouve *et al.* 2015, figs 2, 4, 15). The teeth of *Megadontosuchus* are all enlarged and represent an apomorphic morphology for a tomistomine (Piras *et al.* 2007, fig. 2). The dentition of *T. schlegelii* is homodont with only the 5th maxillary tooth being larger, and almost constant spacing along the tooth row. Similar morphology is also found in *Gavialosuchus* (Toula & Kail 1885, pl. 2), ‘*T.*’ *calaritanum* (Nicholl *et al.* 2020, fig. 14) and ‘*T.*’ *gaudense* (Nicholl *et al.* 2020, fig. 8).

**Postcranial skeleton.** The postcranial region is missing or poorly preserved in many tomistomines, making detailed comparisons difficult. Therefore, only species with well-known postcranial material are used here, including *Maomingosuchus*, *Penghusuchus* (Shan *et al.* 2009, figs 6–14), *Toyotamaphimeia* (Kobayashi *et al.* 2006, figs 31–68), *Thecachampsia carolinensis* (Erickson & Sawyer 1996, figs 7–21) and *T. schlegelii*.

The proatlas of *M. acutirostris* is boomerang-shaped and resembles that of *Penghusuchus* and *Toyotamaphimeia*, but it has a more elongated posterior process and a much higher medial keel. In the other species, like *T. schlegelii*, the proatlas is more block-like. An atlantal rib with a dorsal projection is known only in *Maomingosuchus* and *Toyotamaphimeia*.

In *M. acutirostris*, *Thecachampsia carolinensis* and *T. schlegelii*, the scapular blade is broad, whereas it is narrower in *Toyotamaphimeia* and even wider in *Penghusuchus*. The coracoid foramen in *M. acutirostris* is much smaller than that of *Toyotamaphimeia*, *Thecachampsia carolinensis* and *T. schlegelii*. The iliac blade of *M. acutirostris* is slightly distorted, but relatively broad with a shallow dorsal indentation, similar to *T. schlegelii*. *Toyotamaphimeia* has a narrower iliac blade and a shallower dorsal indentation. In *Penghusuchus* the dorsal indentation is very small, and in *Thecachampsia carolinensis* the posterior part of the blade seems to be sloped. Anteriorly, a prominent process is visible on the ilium of *M. acutirostris*. The process is visible, but smaller than in *Toyotamaphimeia* and *Penghusuchus*. No such process is visible in *T. schlegelii* or *Thecachampsia carolinensis*. Besides *M. acutirostris*, *Toyotamaphimeia* and *Penghusuchus*, such a process is known in gharials.

The dorsal osteoderms of *M. acutirostris*, *T. schlegelii* and *Toyotamaphimeia* have a prominent dorsal keel,

whereas no keel is present in *Penghusuchus* or *Thecachampsia carolinensis*.

## Comparative discussion

*Maomingosuchus* differs from other tomistomines in general snout shape, but the sizes and snout-to-skull ratios are almost similar. Only in *Maomingosuchus acutirostris* is the snout much broader at the level of the 5th maxillary tooth and similar to *Marccosuchus*. Both of these species also have large teeth (see below) that could indicate a more generalist lifestyle.

The size ratio between the supratemporal fenestra and the orbit differs between *M. acutirostris* and other *Maomingosuchus* specimens. However, the size difference in the supratemporal fenestrae between *Maomingosuchus* specimens is not large, but represents the only synapomorphy in the phylogenetic analysis that unites *Maomingosuchus petrolicus* + Krabi-*Maomingosuchus*. This ratio seems to be variable between other tomistomine taxa. For ch. 244 (ratio of the anteroposterior length of the supratemporal fenestra to the anteroposterior length of the orbit: <0.5 [0], 0.5–0.75 [1] or >0.75 [2]); half of the tomistomine taxa were scored with state (1) whereas the other half were scored with state (2). The variability of this character within Tomistominae challenges the synapomorphy of *M. petrolicus* + Krabi-*Maomingosuchus*.

In most tomistomines, the intersupratemporal bar is very narrow in comparison with the width of the skull table. In *M. acutirostris* the ratio is slightly different and the bar is broader compared to other *Maomingosuchus* specimens, but the difference is not that large (for more information see [Supplemental material S2](#)).

In *M. acutirostris* and *M. petrolicus* the 1st dentary tooth perforates the premaxilla anterior to the external naris (unknown for Krabi-*Maomingosuchus*) and this could either be autapomorphic for *Maomingosuchus* or synapomorphic for *M. acutirostris* + *M. petrolicus*.

In *M. petrolicus* and Krabi-*Maomingosuchus* overall tooth size is uniform and the teeth are slender and pointed, as in most tomistomines, but some teeth are more robust and blunter in *M. acutirostris* similar to *Marccosuchus*. This may indicate a somewhat different lifestyle for *M. acutirostris* with a less exclusive piscivorous diet.

*M. acutirostris* and *M. petrolicus* have a thin lamina of the exoccipital projecting ventrally to cover the entrance of the cranio-quadrate passage on the exoccipital, similar to *Gavialis gangeticus* (Gmelin, 1789). This lamina could either be a synapomorphy uniting *M.*

*acutirostris* with *M. petrolicus* or it could be an autapomorphy for the whole genus, depending on the condition in Krabi-*Maomingosuchus*. Determination of the condition in *Penghusuchus* is needed to check if the structure present there is homologous to the condition in *Maomingosuchus*.

## Phylogenetic analysis

### Results

For the maximum parsimony analysis of the traditional search, a total of 17,496 equally optimal trees with lengths of 1017 steps, a consistency index (CI) of 0.317 and a retention index (RI) of 0.690 were recovered ([Figs 15, 16](#)). For the New Technology search analysis, a total of 864 equally optimal trees with the same lengths and same consistency and retention indices were found, and there are no differences in the tree topologies between the results of the traditional and the New Technology search approaches.

Two taxa (*Kentisuchus astrei* Jouve, 2016 and *Melitosaurus*) were pruned from the strict consensus tree after the analysis, because of their unstable positions in the tree. Their potential positions are indicated by the letters 'a' or '> a' for *K. astrei* and '> b' for *Melitosaurus* ([Fig. 16](#)): 'a' indicates that the taxa, if included on the tree, would be sister taxon to a single other taxon, whereas '> a' and '> b' mean that those taxa would be in a polytomy. If *K. astrei* is not pruned from the tree, the resolution is reduced at the base of Tomistominae, whereas the inclusion of *Melitosaurus* leads to a significant loss of resolution among more derived taxa. A complete tree with all of the taxa included can be found in [Supplemental material S2](#).

Overall, the consensus tree is consistent with previous analyses (e.g. Brochu 1999, 2011; Jouve *et al.* 2015; Shan *et al.* 2017; Martin *et al.* 2019; Massonne *et al.* 2019; Nicholl *et al.* 2020), but compared to the analyses of Jouve *et al.* (2015), Shan *et al.* (2017) and Iijima *et al.* (2018), our tree resolution is lower within some groups (Gavialoidea, *Borealosuchus* spp. and Crocodyloidea).

*Maomingosuchus* is monophyletic with *M. petrolicus* from Maoming and Krabi-*Maomingosuchus* forming the sister group to *M. acutirostris*. *Maomingosuchus* was recovered in a basal position within Tomistominae as the sister clade to *Tomistoma* + *Paratomistoma* + *Gavialosuchus* + *Melitosaurus*. A list of synapomorphies can be found in [Supplemental material S2](#).

Bremer support and bootstrap values on the tree are generally low. The Bremer support for Tomistominae is 1. This is also the case for *Maomingosuchus* and *M.*

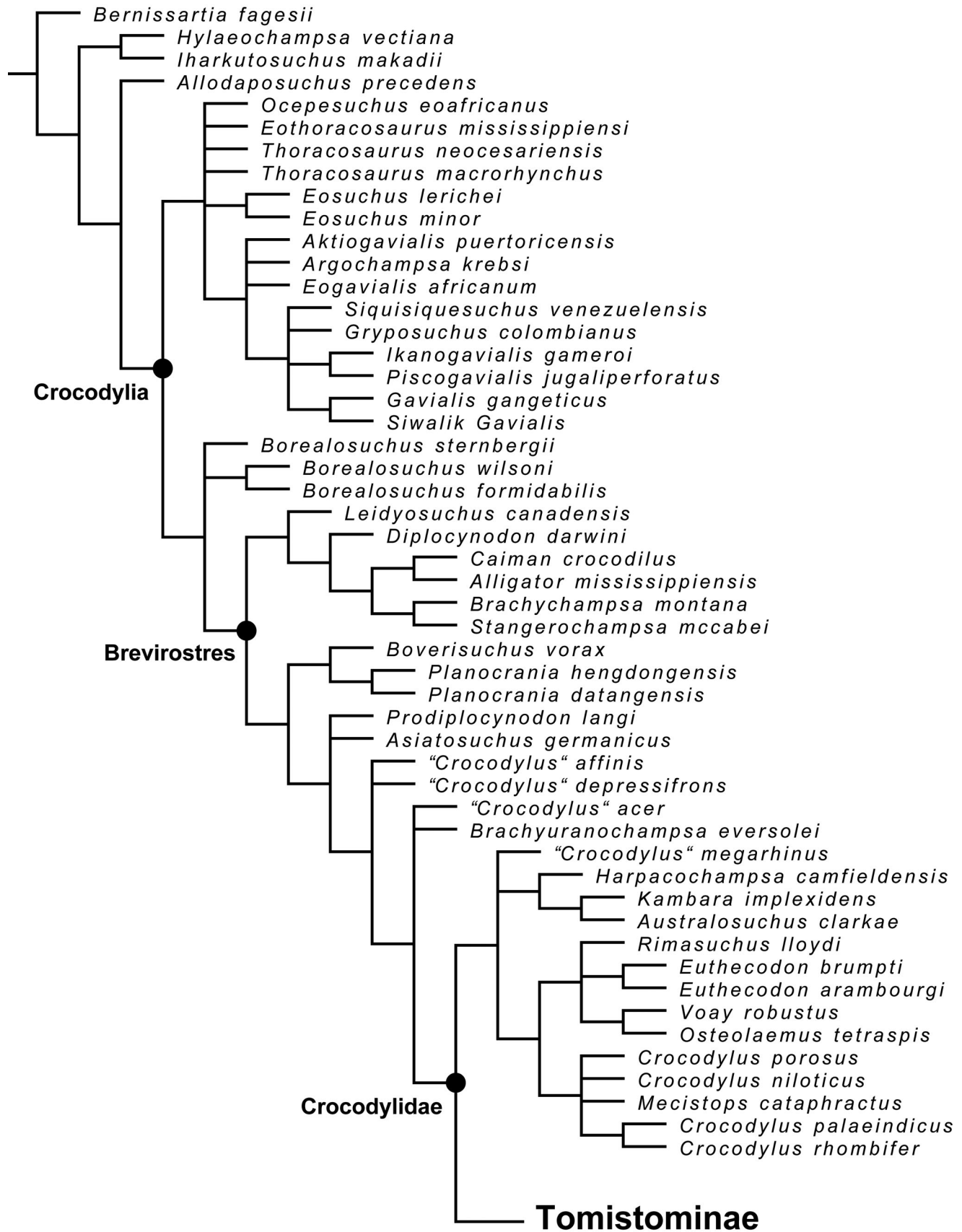


**Figure 15.** Reduced strict consensus tree of 17,496 equally optimal trees, obtained from the maximum parsimony analysis of 72 taxa and 244 characters; tree length = 1017 steps; consistency index = 0.317; and retention index = 0.690.

*petrolicus* + Krabi-*Maomingosuchus* (all Bremer support values can be found in Supplemental material S2). In Tomistominae the frequency differences (GC) standard bootstrap values are 15 for Tomistominae and 18 for *Maomingosuchus*. *M. petrolicus* + Krabi-*Maomingosuchus* have a support of 2.

### Phylogenetic discussion

Outside Tomistominae, the tree is mostly consistent with previous analyses based on morphological data alone (e.g. Brochu 1999, 2011; Jouve *et al.* 2015; Shan *et al.* 2017; Martin *et al.* 2019; Massonne *et al.* 2019; Nicholl *et al.* 2020), but lacks resolution at some nodes (Gavialoidea, *Borealosuchus* spp. and Crocodyloidea) as is also the case in Nicholl *et al.* (2020). This is different in Shan *et al.* (2017) and Iijima *et al.* (2018), most likely due to our ordering of characters (see Materials and methods, above). This ordering also affects tomistomines, in that *Dollosuchoidea* is considered to be the sister taxon to *Thecachampsia antiqua* + *Thecachampsia carolinensis* + *Penghusuchus* + *Toyotamaphimeia* instead of being placed in a more basal position on the tree.

Our analysis yields a polytomy at the base of Tomistominae including *Marccosuchus*, *Kentisuchus astrei*, *Kentisuchus spenceri* and *Megadontosuchus* or a polytomy between *Marccosuchus* and *K. spenceri* if *K. astrei* is pruned from the tree.

*Maomingosuchus* consists of *Maomingosuchus acutirostris*, *Maomingosuchus petrolicus* and the Krabi-*Maomingosuchus* and is supported by three

autapomorphies, a flush margin of the orbit with the skull surface (103–0), a ventral border of the exoccipital convex and ventrally projected (166–0) and a frontal ending at the same level as the anterior extension of the prefrontal (171–1).

The monophyly of *Maomingosuchus* is the most parsimonious hypothesis and found in all trees, despite the weak Bremer support.

In previous analyses (Shan *et al.* 2017; Iijima *et al.* 2018; Nicholl *et al.* 2020), *M. petrolicus* was found in varying positions among tomistomines, but usually in a more derived position than in our current analysis. Only Piras *et al.* (2007) obtained similar results. Only the analysis by Martin *et al.* (2019) included *M. petrolicus* as well as Krabi-*Maomingosuchus* and found *Maomingosuchus* as the sister clade to the extant *T. schlegelii*.

Our rescoring of some characters for *M. petrolicus* and Krabi-*Maomingosuchus* (Supplemental material S2), as well as the incorporation of *M. acutirostris*, results in a more basal position of *Maomingosuchus* that is more congruent with its upper Eocene–lower Oligocene age.

It is noteworthy that the position of *Maomingosuchus* is generally stable on the tree. The genus always forms the sister clade to a group consisting of ‘*Tomistoma*’ *cairensis* + ‘*Tomistoma*’ *coppensi* + *Paratomistoma* + *Tomistoma schlegelii* + ‘*Tomistoma*’ *lusitanica* + *Gavialosuchus* + ‘*Tomistoma*’ *gaudense* + ‘*Tomistoma*’ *calaritanum* + *Melitosaurus*, regardless of whether *K. astrei* or *Melitosaurus* are pruned from the tree or not.

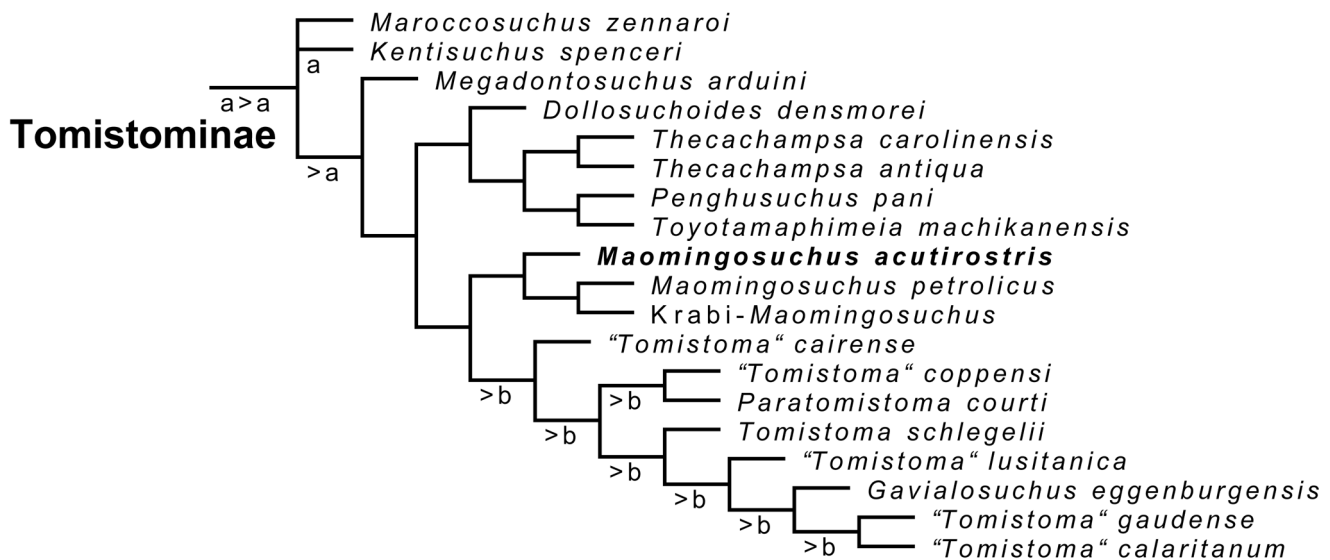


**Figure 16.** Tomistominae phylogeny as inferred from the reduced strict consensus tree of 17,496 equally optimal trees, obtained from the maximum parsimony analysis of 72 taxa and 244 characters; tree length = 1017 steps; consistency index = 0.317; and retention index = 0.690. ‘a’ indicates the alternative position of the pruned *Kentisuchus astrei*. ‘b’ indicates the alternative position of the pruned *Melitosaurus champsoides*.

A new phylogenetic analysis by Rio & Mannion (2021) recovered *Gavialis* as more closely related to *Tomistoma* than to other extant crocodylians, based solely on morphological data. This further suggests paraphyly of the classical subfamily Tomistominae. However, the more basal position of *M. petrolicus* is also supported in this analysis, indicating that *Maomingosuchus* belongs to a stem group leading to recent *Tomistoma* and *Gavialis*. Further analyses that include *M. acutirostris* and *Krabi-Maomingosuchus* are necessary to get better insights into the relationships between *Maomingosuchus* and other gavialoids.

### Palaeobiogeographical implications

Based on our analysis and previous phylogenies most basal tomistomine taxa are from the western Tethyan region. It is therefore most parsimonious to assume that they originated in that area before the early Eocene (as already proposed by Jouve *et al.* 2015; Jouve 2016; Shan *et al.* 2017; Iijima *et al.* 2018; Nicholl *et al.* 2020). Moreover, based on our analysis, we conclude that dispersals towards eastern Asia must have happened multiple times independently. Accordingly, the first dispersal occurred no later than the late Eocene for the

stem lineage of *Maomingosuchus*, while a second dispersal occurred no later than the early–middle Miocene for the stem lineage of *Penghusuchus* + *Toyotamaphimeia*, and a third one took place for the stem lineage of the extant *Tomistoma schlegelii* during the Neogene. For better clarification, we mapped the ages of the respective fossils based on available data from the literature onto our phylogenetic tree (Fig. 17).

Based on palaeogeographical reconstructions, two different dispersal routes for the stem lineage of *Maomingosuchus* seem possible: an eastern route from Europe via coastal dispersal along the Neotethys to south-eastern Asia (consistent with Jouve *et al.* 2015, fig. 18) and a western route from Europe via North America and Beringia to south-eastern Asia. The latter one as suggested for Orientalosuchina (Massonne *et al.* 2019) seems rather unlikely, due to the absence of suitable fossils in North America at that time.

A potential key to solve this problem are the tomistomine species from the middle Eocene of central and south Asia, but their tomistomine affinities have been questioned (Jouve 2004; Jouve *et al.* 2015). ‘*Tomistoma*’ *borisovi* Efimov, 1988 and *Dollosuchus zajsanicus* (Efimov, 1982) are only fragmentary and difficult to diagnose (Piras *et al.* 2007; Jouve *et al.* 2015; Kuzmin & Zvonok 2021). ‘*Tomistoma*’ *tandoni* Sahni & Mishra, 1975 is known only from a mandible and

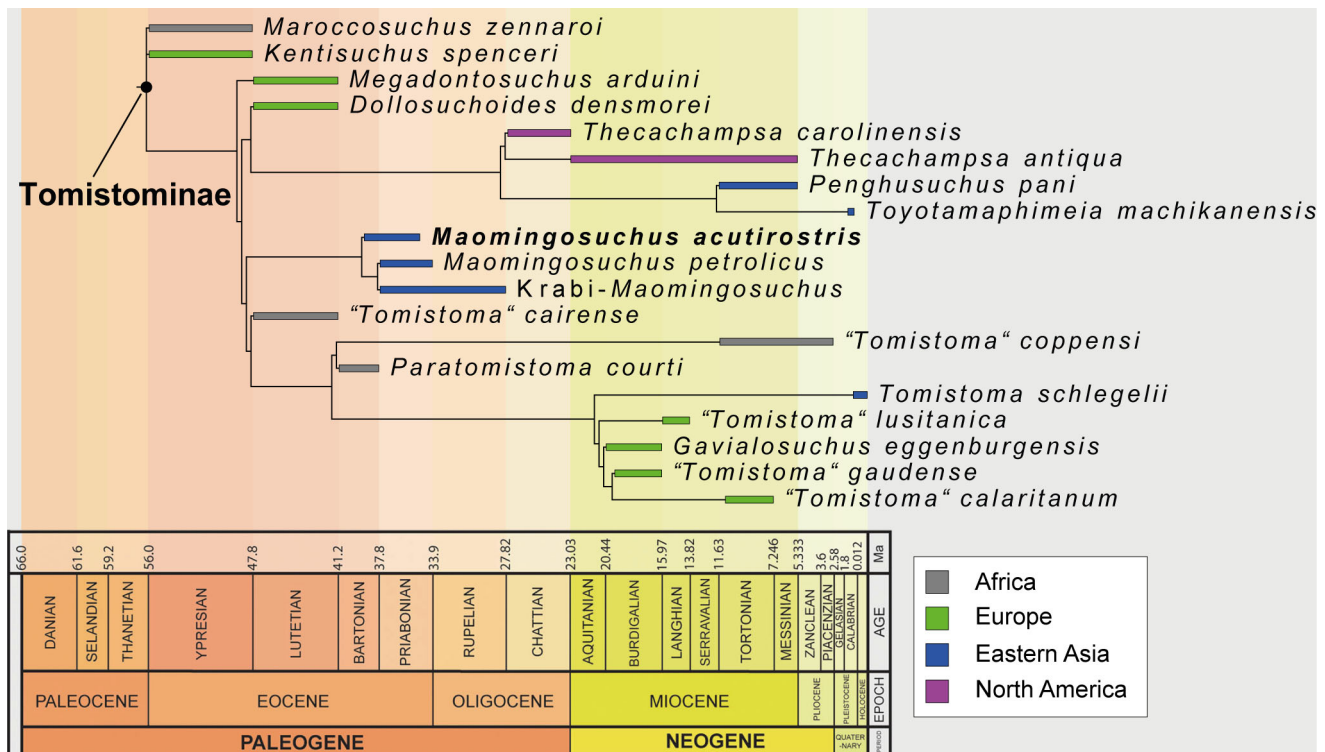


**Figure 17.** Time-scaled reduced strict consensus tree of Tomistominae, based on available data from the literature. *Kentisuchus astrei* and *Melitosaurus champsoides* pruned (modified after Nicholl *et al.* 2020).

*Ferganosuchus planus* Efimov, 1982 from a skull table and some postcranial material. Further crocodylian remains are known from the middle Eocene Pondaung Formation of central Myanmar (Tsubamoto *et al.* 2006a, b), including two different crocodylian teeth figured by Tsubamoto *et al.* (2006b, fig. 12) of which the larger one resembles the larger teeth of *Maomingosuchus acutirostris* in exhibiting a well-developed lateral edge. According to Tsubamoto *et al.* (2006a), there are more teeth and bone fragments from the same locality, but they remain unpublished.

The results of the current phylogenetic analysis, together with previous analyses (Martin & Lauprasert 2010; Skutschas *et al.* 2014; Shan *et al.* 2017, 2021; Martin *et al.* 2019; Massonne *et al.* 2019) demonstrate a close connection between the crocodylian faunas of three east Asian fossil sites: the Na Duong Basin in Vietnam (e.g. Böhme *et al.* 2011, 2013; Wysocka *et al.* 2020), the Maoming Basin in China (e.g. Jin 2008; Averianov *et al.* 2016) and the Wai-Lek from Krabi Province, Thailand (e.g. Benammi *et al.* 2001; Claude *et al.* 2007). In all three localities, similar crocodylians of two unrelated groups are found that, based on their morphology, occupied different niches, with the longirostrine *Maomingosuchus* more piscivorous (Shan *et al.* 2017; Martin *et al.* 2019), and the brevirostrine *Orientalosuchina* with a more generalist diet (Martin & Lauprasert 2010; Skutschas *et al.* 2014; Wang *et al.* 2016; Li *et al.* 2019; Massonne *et al.* 2019; Shan *et al.* 2021).

Dispersal towards eastern Asia, however, probably differed for both groups. While *Orientalosuchina* were already present in the region during the Late Cretaceous (Li *et al.* 2019) and most likely originated in North America (Massonne *et al.* 2019), the stem lineage of *Maomingosuchus* probably arrived in eastern Asia from Europe sometime before the upper Eocene (e.g. Jouve *et al.* 2015; Shan *et al.* 2017; Martin *et al.* 2019).

The crocodylian faunas of the three localities (Na Duong, Maoming and Krabi) are very similar, but show distinct species, which could be explained by either climatic and/or geographical barriers. Climatic barriers between the Na Duong and Maoming basins seem unlikely, since both basins are close to each other (~400 km apart) and at the same latitude (Fig. 1). This distribution recalls a similar case in the turtle fauna with *Banhxeochelys trani* Garbin, Böhme & Joyce, 2019 from Na Duong being closely related to *Isometremys lacuna* Chow & Yeh, 1962 and *Guangdongemys pingi* Claude, Zhang, Li, Mo, Kuang & Tong, 2012 from Maoming (Garbin *et al.* 2019). Based on the presence of closely related crocodile and turtle faunas in Na Duong, Maoming and Krabi, it seems likely that other

middle–upper Eocene deposits in eastern and south-eastern Asia (e.g. the Pondaung Formation in Myanmar) will yield species of *Maomingosuchus* and *Orientalosuchina*. Further investigations on those fossil sites are needed to obtain more information of the faunas and palaeobiogeography of eastern and south-eastern Asia during the upper Eocene–lower Oligocene.

## Conclusions

*Maomingosuchus acutirostris* sp. nov. is a new tomistomine species from the middle–upper Eocene deposits (late Bartonian–Priabonian age, 39–35 Ma) of the Na Duong Basin in Vietnam. *M. acutirostris* is a medium-sized tomistomine with a relatively robust snout and multiple enlarged teeth, similar to *Maroccosuchus*, potentially indicating a less piscivorous diet than the extant *Tomistoma schlegelii*.

Our phylogenetic analysis recovers *M. acutirostris* as the sister taxon to a monophyletic group consisting of *M. petrolicus* from the upper Eocene of the Maoming Basin of south-eastern China and Krabi-*Maomingosuchus* from the upper Eocene–lower Oligocene of Wai-Lek from Krabi Province, Thailand. The basal position of *Maomingosuchus* is generally stable on the tree, being congruent with the upper Eocene–lower Oligocene age of *Maomingosuchus*.

The phylogenetic analysis supports a western Tethyan origin for tomistomines with three independent dispersal events from Europe to eastern Asia. One for the stem lineage of *Maomingosuchus*, another for the stem lineage of *Pengusuchus* + *Toyotamaphimeia* and a third for the stem lineage of the extant *T. schlegelii*.

The similarities between the crocodile faunas of Na Duong, Maoming and Krabi are noteworthy. More material from other upper Eocene–lower Oligocene sites in eastern Asia could show if representatives of *Maomingosuchus* and *Orientalosuchina* were more widely spread across east Asia than currently known and could shed new light on the palaeobiogeographical and faunal connections between these different Eocene–Oligocene localities in eastern Asia.

## Acknowledgements

We want to thank the editor Jonah Choiniere and two anonymous reviewers for their comments, which helped us improve the manuscript. We thank our Vietnamese colleagues who facilitated and participated in the Na Duong palaeontological expeditions of 2009, 2011 and 2012: Nguyễn Việt Hưng, La Thế Phúc, Đặng Ngọc

Trần, Đỗ Đức Quang, Phan Đồng Pha. The authors further wish to thank Ivan Kuzmin (University of Saint Petersburg), Gustavo Darlim, Josephina Hartung, Panagiotis Kampouridis, Thomas Lechner, Márton Rabi, Adrian Tröscher and Jules Walter (all University of Tübingen) for discussions. Agnes Fatz and Wolfgang Gerber are thanked for helping with photographing the material in Figures 2, 3 and 6; Regina Ellenbracht and Henrik Stöhr (both University of Tübingen) are thanked for preparation. Christopher A. Brochu (University of Iowa) is thanked for stimulating discussion during his visit to Tübingen and for photographs of the *Maomingosuchus petrolicus* holotype and Krabi-*Maomingosuchus*. Sonja Scheiben and Adrian Tröscher (University of Tübingen) kindly provided us with photographs of extant crocodile material for comparisons. Ingmar Werneburg (University of Tübingen) and Alexander Kupfer (Staatliches Museum für Naturkunde Stuttgart) are thanked for granting access to specimens under their care. The Willi Hennig Society is thanked for providing access to the software TNT v. 1.5.

## Supplemental material

Supplemental material for this article can be accessed here: <https://doi.org/10.1080/14772019.2022.2054372>.

## ORCID

Tobias Massonne  <http://orcid.org/0000-0002-6782-5280>

Felix J. Augustin  <http://orcid.org/0000-0002-7787-5601>

## References

- Antunes, M. T.** 1961. *Tomistoma lisitanica*, crocodilien du Miocène du Portugal. *Revista Faculdade de Ciências da Universidade de Lisboa (Series 2)*, **9**, 5–88.
- Averianov, A., Obratzsova, E., Danilov, I., Skutschas, P. & Jin, J.** 2016. First nimravid skull from Asia. *Scientific Reports*, **6**(1), 25812. doi:10.1038/srep25812
- Benammi, M., Chaimanee, Y., Jaeger, J. J., Suteethorn, V. & Ducrocq, S.** 2001. Eocene Krabi Basin (southern Thailand): paleontology and magnetostratigraphy. *Geological Society of America Bulletin*, **113**(2), 265–273.
- Benton, M. J. & Clark, J. M.** 1988. Archosaur phylogeny and the relationships of the Crocodylia. Pp. 295–338 in M. J. Benton (ed.) *The phylogeny and classification of the tetrapods, volume 1, amphibians, reptiles, birds*. Clarendon Press, Oxford.
- Berg, D. E.** 1969. *Charactosuchus kugleri*, eine neue Krokodilart aus dem Eozän von Jamaica. *Eclogae Geologicae Helvetiae*, **62**, 731–735.
- Bezuijen, M. R., Shwedick, B. M., Sommerlad, R., Stevenson, C. & Steubing, R. B.** 2010. *Tomistoma Tomistoma schlegelii*. Pp. 133–138 in Crocodile Specialist Group (eds) *Crocodile: status survey and conservation action plan*. IUCN, Darwin.
- Böhme, M., Prieto, J., Schneider, S., Hung, N. V. & Tran, D. N.** 2011. The Cenozoic on-shore basins of northern Vietnam: biostratigraphy, vertebrate and invertebrate faunas. *Journal of Asian Earth Sciences*, **40**(2), 672–687.
- Böhme, M., Aiglstorfer, M., Antoine, P. O., Appel, E., Havlik, P., Métails, G., Phug, L. T., Schneider, S., Setzer, F., Tappert, R., Tran, D. N., Uhl, D. & Prieto, J.** 2013. Na Duong (northern Vietnam) – an exceptional window into Eocene ecosystems from southeast Asia. *Zitteliana A*, **53**, 121–167.
- Brochu, C. A.** 1999. Phylogenetics, taxonomy, and historical biogeography of Alligatoroidea. *Memoirs of the Society of Vertebrate Paleontology*, **6**, 9–100.
- Brochu, C. A.** 2003. Phylogenetic approaches toward crocodylian history. *Annual Review of Earth and Planetary Sciences*, **31**(1), 357–397.
- Brochu, C. A.** 2007. Systematics and taxonomy of Eocene tomistomine crocodylians from Britain and Northern Europe. *Palaeontology*, **50**(4), 917–928.
- Brochu, C. A.** 2011. Phylogenetic relationships of *Necrosuchus ionensis* Simpson, 1937 and the early history of caimanines. *Zoological Journal of the Linnean Society*, **163**(supplement 1), S228–S256.
- Brochu, C. A. & Gingerich, P. D.** 2000. New tomistomine crocodylian from the middle Eocene (Bartonian) of Wadi Hitan, Fayum Province, Egypt. *Contributions from the Museum of Paleontology, University of Michigan* **30**, 251–268.
- Buckland, W.** 1836. *Geology and mineralogy considered with reference to natural theology*. W. Pickering, London, 618 pp.
- Buscalioni, A. D., Ortega, F. & Vasse, D.** 1997. New crocodiles (Eusuchia: Alligatoroidea) from the Upper Cretaceous of southern Europe. *Comptes Rendus de l'Académie des Sciences, Series IIA, Earth and Planetary Science*, **325**(7), 525–530.
- Capellini, G.** 1890. Sul cocodrilliano garialoide (*Tomistoma calaritanus*) scoperto nella collina di Cagliari nel 1868. *Atti della Reale Accademia Lincei, Memorie della Classe di Scienze Fisiche, Matematiche e Naturali, serie 4*, **6**, 507–533.
- Chow, M. C. & Yeh, H. K.** 1962. A new emydid from Eocene of Maoming Kwangtung. *Vertebrata Palasiatica*, **6**(3), 225–229.
- Clark, J. M. & Norell, M.** 1992. The Early Cretaceous crocodylomorph *Hylaeochampsia vectiana* from the Wealden of the Isle of Wight. *American Museum Novitates*, **3032**, 1–19.
- Claude, J., Suteethorn, V. & Tong, H.** 2007. Turtles from the late Eocene–early Oligocene of the Krabi Basin (Thailand). *Bulletin de la Société géologique de France*, **178**(4), 305–316.
- Claude, J., Zhang, J. Y., Li, J. J., Mo, J. Y., Kuang, X. W. & Tong, H.** 2012. Geoemydid turtles from the Late Eocene Maoming basin, southern China. *Bulletin de la Société géologique de France*, **183**(6), 641–651.

- Cossette, A. P. & Brochu, C. A.** 2018. A new specimen of the alligatoroid *Bottosaurus harlani* and the early history of character evolution in alligatorids. *Journal of Vertebrate Paleontology*, **38**(4), 1–22.
- Darlim, G., Lee, M. S. Y., Walter, J. & Rabi, M.** 2022. The impact of molecular data on the phylogenetic position of the putative oldest crown crocodylian and the age of the clade. *Biology Letters*, **18**, 20210603. doi:10.1098/rsbl.2021.0603
- Delfino, M., Codrea, V., Folie, A., Dica, P., Godefroit, P. & Smith, T.** 2008. A complete skull of *Allodaposuchus precedens* Nopcsa, 1928 (Eusuchia) and a reassessment of the morphology of the taxon based on the Romanian remains. *Journal of Vertebrate Paleontology*, **28**(1), 111–122.
- de Zigno, A.** 1880. Sopra un cranio di coccodrillo scoperto nel terreno eoceno del Veronese. *Atti della Reale Accademia Nazionale dei Lincei: Memorie della Classe di Scienze fisiche, Matematiche e Naturale, Serie 3*(5), 65–72.
- Dollo, L.** 1883. Première note sur les crocodyliens de Bernissart. *Bulletin du Musée royal d'Histoire naturelle de Belgique*, **2**, 309–338.
- Efimov, M. B.** 1982. New fossil crocodiles from the USSR. *Paleontologičeskij žurnal*, **2**, 146–150.
- Efimov, M. B.** 1988. Fossil crocodiles and champsosaurs of Mongolia and the USSR. *Trudy Sovmestnoi Sovetskogo-Mongol'skoi Paleontologičeskoi Ekspeditsii*, **36**, 1–108.
- Erickson, B. R. & Sawyer, G. T.** 1996. The estuarine crocodile *Gavialosuchus carolinensis* n. sp. (Crocodylia: Eusuchia) from the late Oligocene of South Carolina, North America. *Science Museum of Minnesota Monographs (Paleontology)*, **3**, 1–49.
- Fitzinger, L. J.** 1826. *Neue Classification der Reptilien nach ihren natürlichen Verwandtschaften. Nebst einer Verwandtschaftstafel und einem Verzeichnisse der Reptiliensammlung des K.K. zoologischen Museum's zu Wien.* J. G. Heubner, Vienna, 66 pp.
- Garbin, C. G., Böhme, M. & Joyce, W. G.** 2019. A new testudinoid turtle from the Middle to late Eocene of Vietnam. *PeerJ*, **7**(1), e6280. doi:10.7717/peerj.6280
- Gmelin, J. F.** 1789. Regnum animale. Pp. 1033–1516 in *Caroli a Linne Systema Naturae per regna tri naturae, secundum classes, ordines, genera, species, cum characteribus, differentiis, synonymis, locis. volume 1.* G. E. Beer, Leipzig.
- Goloboff, P. A., Farris, J. S. & Nixon, K. C.** 2008. TNT, a free program for phylogenetic analysis. *Cladistics*, **24**(5), 774–786.
- Goloboff, P. A. & Catalano, S. A.** 2016. TNT version 1.5, including a full implementation of phylogenetic morphometrics. *Cladistics*, **32**(3), 221–238.
- Hulke, J. W.** 1871. Note on some reptilian fossils from Gozo. *Quarterly Journal of the Geological Society of London*, **27**(1–2), 29–33.
- Huxley, T. H.** 1875. On *Stagonolepis robertsoni*, and on the evolution of the Crocodylia. *Quarterly Journal of the Geological Society of London*, **31**(1–4), 423–438.
- Iijima, M., Momohara, A., Kobayashi, Y., Hayashi, S., Ikeda, T., Taruno, H., Watanabe, K., Tanimoto, M. & Furui, S.** 2018. *Toyotamaphimeia* cf. *machikanensis* (Crocodylia, Tomistominae) from the middle Pleistocene of Osaka, Japan, and crocodylian survivorship through the Pliocene-Pleistocene climatic oscillations. *Palaeogeography, Palaeoclimatology, Palaeoecology*, **496**, 346–360.
- Iijima, M. & Kobayashi, Y.** 2019. Mosaic nature in the skeleton of East Asian crocodylians fills the morphological gap between “Tomistominae” and Gavialinae. *Cladistics*, **35**(6), 623–632.
- Jin, J. H.** 2008. On the age of the Youganwo Formation in the Maoming basin, Guangdong Province. *Journal of Stratigraphy*, **32**(1), 47–50.
- Jonet, S. & Wouters, G.** 1972. Présence d'un crocodyliens nouveau dans les phosphates Yprésiens du Maroc. *Bulletin de la Société Belge de Géologie, de Paléontologie et d'Hydrologie*, **81**, 209–210.
- Jonet, S. & Wouters, G.** 1977. *Marccosuchus zennaroi*, crocodylian Eusuchien nouveau des Phosphates du Maroc. Notes et Mémoires du Service Géologique du Maroc, **38**, 177–202.
- Jouve, S.** 2004. *Etude des Crocodyloformes fini Crétacé-Paléogène du Bassin des Oulad Abdoun (Maroc) et comparaison avec les faunes africaines contemporaines: systématique, phylogénie et paléobiogéographie.* Unpublished PhD thesis, Muséum National d'Histoire Naturelle, Paris, 651 pp.
- Jouve, S.** 2016. A new basal tomistomine (Crocodylia, Crocodyloidea) from Issel (Middle Eocene; France): palaeobiogeography of basal tomistomines and palaeogeographic consequences. *Zoological Journal of the Linnean Society*, **177**(1), 165–182.
- Jouve, S., Bouya, B., Amaghazaz, M. & Meslouh, S.** 2015. *Marccosuchus zennaroi* (Crocodylia: Tomistominae) from the Eocene of Morocco: phylogenetic and palaeobiogeographical implications of the basalmost tomistomine. *Journal of Systematic Palaeontology*, **13**(5), 421–445.
- Kälin, J. A.** 1955. Zur Stammesgeschichte der Crocodylia. *Revue Suisse de Zoologie*, **62**, 347–356.
- Kobatake, N., ChiJi, M., Ikebe, N., Ishida, S., Kamei, T., Nakaseko, K. & Matsumoto, E.** 1965. Discovery of crocodile fossil from the Osaka Group. *The Quaternary Research (Daiyonki-Kenkyu)*, **4**(2), 49–58.
- Kobayashi, Y., Tomida, Y., Kamei, T. & Eguchi, T.** 2006. Anatomy of a Japanese tomistomine crocodylian, *Toyotamaphimeia machikanensis* (Kamei et Matsumoto, 1965), from the middle Pleistocene of Osaka Prefecture: the reassessment of its phylogenetic status within Crocodylia. *National Science Museum Monographs*, **35**, 1–121.
- Kuzmin, I. T. & Zvonok, E. A.** 2021. Crocodylian assemblage from the middle Eocene Ikovo locality (Lugansk Province, Ukraine), with a discussion of the fossil record and geographic origins of crocodyliform fauna in the Paleogene of Europe. *Geobios*, **65**, 7–27. doi: 10.1016/j.geobios.2021.02.002
- Laurenti, J. N.** 1768. *Specimen medicum, exhibens synopsis reptilium emendatam cum experimentis circa venena et antidota reptilium austracorum, quod auctoritate et consensu.* J. Thomae, Vienna, 217 pp.
- Lee, M. S. Y. & Yates, A. M.** 2018. Tip-dating and homoplasy: reconciling the shallow molecular divergences of modern gharials with their long fossil record. *Proceedings of the Royal Society B*, **285**, 20181071. doi: 10.1098/rspb.2018.1071

- Leidy, J.** 1852. Description of a new species of crocodile from the Miocene of Virginia. *Journal of the Academy of Natural Sciences of Philadelphia*, **2**, 135–138.
- Li, C., Wu, X. C. & Rufolo, S. J.** 2019. A new crocodyloid (Eusuchia: Crocodylia) from the Upper Cretaceous of China. *Cretaceous Research*, **94**, 25–39.
- Li, J. L.** 1975. New material on *Tomistoma petrolicus* of Maoming, Guangdong. *Vertebrata Palasiatica*, **13**(3), 190–194.
- Lucas, S. G., & Estep, J. W.** 2000. Osteology of *Allognathosuchus mooki* Simpson, a Paleocene crocodylian from the San Juan Basin, New Mexico, and the monophyly of *Allognathosuchus*. *New Mexico Museum of Natural History and Science Bulletin*, **16**, 155–168.
- Marsh, O. C.** 1871. Notice of some new fossil reptiles from the Cretaceous and Tertiary formations. *American Journal of Science (Series 3)*, **1**(6), 447–459.
- Martin, J. E.** 2007. New material of the Late Cretaceous globidontan *Acynodon iberoccitanus* (Crocodylia) from southern France. *Journal of Vertebrate Paleontology*, **27**(2), 362–372.
- Martin, J. E., & Lauprasert, K.** 2010. A new primitive alligatorine from the Eocene of Thailand: relevance of Asiatic members to the radiation of the group. *Zoological Journal of the Linnean Society*, **158**(3), 608–628.
- Martin, J. E., Delfino, M., Garcia, G., Godefroit, P., Berton, S. & Valentin, X.** 2016. New specimens of *Allodaposuchus precedens* from France: intraspecific variability and the diversity of European Late Cretaceous eusuchians. *Zoological Journal of the Linnean Society*, **176**(3), 607–631.
- Martin, J. E., Lauprasert, K., Tong, H., Suteethorn, V. & Buffetaut, E.** 2019. An Eocene tomistomine from peninsular Thailand. *Annales de Paléontologie*, **105**(3), 245–253.
- Massonne, T., Vasilyan, D., Rabi, M. & Böhme, M.** 2019. A new alligatoroid from the Eocene of Vietnam highlights an extinct Asian clade independent from extant *Alligator sinensis*. *PeerJ*, **7**, e7562. doi:10.7717/peerj.7562
- Meyer, H. von.** 1832. *Paleologia zur Geschichte der Erde und ihrer Geschöpfe*. S. Schmerber, Frankfurt am Main, 560 pp.
- Mook, C. C.** 1921. Description of a skull of a Bridger Crocodylian. *Bulletin of the American Museum of Natural History*, **44**, 111–116.
- Mook, C. C.** 1941. A new crocodylian from the Lance Formation. *American Museum Novitates*, **1128**, 1–5.
- Müller, L.** 1927. Ergebnisse der Forschungsreisen Prof. E. Stromers in den Wüsten Ägyptens. V. Tertiär Wirbeltiere. 1. Beiträge zur Kenntnis der Krokodilier des ägyptischen Tertiärs. *Abhandlungen der Bayerischen Akademie der Wissenschaften Mathematisch-naturwissenschaftliche Abteilung*, **31**, 1–96.
- Müller, S.** 1838. Waarnemingen over de Indische krokodillen en Beschrijving van eene nieuwe soort. *Tydschrift voor Natuurlijke Geschiedenis en Physiologie*, **5**, 67–87.
- Myrick, A. C.** 2001. *Thecachampsia antiqua* (Leidy, 1852) (Crocodylidae, Thoracosaurinae) from fossil marine deposits at Lee Creek Mine, Aurora, North Carolina, USA. *Smithsonian Contributions to Paleobiology*, **90**, 219–225.
- Nicholl, C. S., Rio, J. P., Mannion, P. D. & Delfino, M.** 2020. A re-examination of the anatomy and systematics of the tomistomine crocodylians from the Miocene of Italy and Malta. *Journal of Systematic Palaeontology*, **18**(22), 1853–1889.
- Nopcsa, F.** 1928. Paleontological notes on Reptilia. 7. Classification of the Crocodylia. *Geologica Hungarica, Series Palaeontologica*, **1**, 75–84.
- Owen, R.** 1849. *A history of British fossil reptiles. Volume 1*. Cassell, London, 657 pp.
- Owen, R.** 1874. Monograph on the fossil Reptilia of the Wealden and Purbeck formations. Supplement 6 (*Hylaeochampsia*). *Monographs of the Palaeontographical Society*, **27**(6), 1–7.
- Pickford, M.** 1994. Late Cenozoic crocodiles (Reptilia: Crocodylidae) from the Western Rift, Uganda. *Geology and Palaeobiology of the Albertine Rift Valley, Uganda-Zaire*, **2**, 137–155.
- Piras, P., Delfino, M., Del Favero, L. & Kotsakis, T.** 2007. Phylogenetic position of the crocodylian *Megadontosuchus arduini* and tomistomine palaeobiogeography. *Acta Palaeontologica Polonica*, **52**(2), 315–328.
- Rio, J. P. & Mannion, P. D.** 2021. Phylogenetic analysis of a new morphological dataset elucidates the evolutionary history of Crocodylia and resolves the long-standing gharial problem. *PeerJ*, **9**, e12094. doi:10.7717/peerj.12094
- Risteovski, J., Price, G. J., Weisbecker, V., & Salisbury, S. W.** 2021. First record of a tomistomine crocodylian from Australia. *Scientific Reports*, **11**(1), 12158. doi:10.1038/s41598-021-91717-y
- Sahni, A. & Mishra, V. P.** 1975. Lower Tertiary vertebrates from western India. *Monographs of the Palaeontological Society of India*, **3**, 1–48.
- Shan, H. Y., Wu, X. C., Cheng, Y. N. & Sato, T.** 2009. A new tomistomine (Crocodylia) from the Miocene of Taiwan. *Canadian Journal of Earth Sciences*, **46**(7), 529–555.
- Shan, H. Y., Wu, X. C., Cheng, Y. N. & Sato, T.** 2017. *Maomingosuchus petrolica*, a restudy of ‘*Tomistoma petrolica*’ Yeh, 1958. *Palaeoworld*, **26**(4), 672–690.
- Shan, H. Y., Wu, X. C., Sato, T., Cheng, Y. N. & Rufolo, S.** 2021. A new alligatoroid (Eusuchia, Crocodylia) from the Eocene of China and its implications for the relationships of Orientalosuchina. *Journal of Paleontology*, **95**(6), 1321–1339.
- Simpson, G. G.** 1930. *Allognathosuchus mooki*, a new crocodile from the Puerco Formation. *American Museum Novitates*, **445**, 1–16.
- Skutschas, P. P., Danilov, I. G., Kodrul, T. M. & Jin, J.** 2014. The first discovery of an alligatorid (Crocodylia, Alligatoroidea, Alligatoridae) in the Eocene of China. *Journal of Vertebrate Paleontology*, **34**(2), 471–476.
- Toula, F. & Kail, J. A.** 1885. Über einen Krokodil-Schädel aus den Tertiärablagerungen von Eggenburg in Niederösterreich: eine paläontologische Studie. *Denkschriften der Kaiserlichen Akademie der Wissenschaften von Wien, Mathematisch-naturwissenschaftliche Klasse*, **50**, 299–355.
- Tsubamoto, T., Egi, N., Takai, M., Shigehara, N., Suzuki, H., Nishimura, T., Ugai, H., Maung, M., Sein, C., Tun, S. T., Soe, A. N., Aung, A. K., Thein, T., Htike, T. & Thein, Z. M. M.** 2006a. A summary of the Pondaung fossil expeditions. *Asian Paleoprimateology*, **4**, 1–66.
- Tsubamoto, T., Egi, N. & Takai, M.** 2006b. Notes on fish, reptilian, and several fragmentary mammalian dental

- fossils from the Pondaung Formation. *Asian Paleoprimatology*, **4**, 98–110.
- Wang, Y. Y., Sullivan, C. & Liu, J.** 2016. Taxonomic revision of *Eoalligator* (Crocodylia, Brevirostres) and the paleogeographic origins of the Chinese alligatoroids. *PeerJ*, **4**, e2356. doi:10.7717/peerj.2356
- Whitaker, R. & Whitaker, N.** 2008. Who's got the biggest? *Crocodile Specialist Group Newsletter*, **27**(4), 26–30.
- Wu, X. C., Brinkman, D. B. & Russell, A. P.** 1996. A new alligator from the Upper Cretaceous of Canada and the relationship of early eusuchians. *Palaeontology*, **39**, 351–376.
- Wysocka, A., Pha, P. D., Durska, E., Czarniecka, U., Thang, D. V., Filipek, A., Cuong, N. Q., Tuan, D. M., Huyen, N. X., Tha, H. V. & Staniszewski, R.** 2020. The Na Duong Basin (North Vietnam): a key for understanding Paleogene basin evolution in relation to the left-lateral Cao Bang-Tien Yen Fault. *Journal of Asian Earth Sciences*, **195**, 104350. doi:10.1016/j.jseas.2020.104350
- Yeh, H. K.** 1958. A new crocodile from Maoming, Kwangtung. *Vertebrata Palasiatica*, **2**(4), 237–242.

**Associate Editors: Jonah Choiniere/Paul Barrett**